

AASERT Grant #N00014-93-1-0827

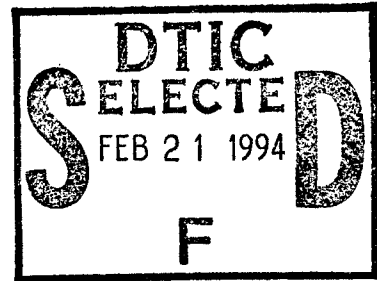
**Third Semi-Annual Progress Report**  
(covering the period of 07/16/94-02/15/95)

**Project Title: Investigation of a Normal Incidence High-  
Performance P-type Strained Layer  
 $In_{0.3}Ga_{0.7}As/In_{0.52}Al_{0.48}As$  Quantum Well  
Infrared Photodetector.**

Submitted to

Max N. Yoder

Office of Naval Research  
Code 3140  
800 North Quincy Street  
Arlington, VA 22217-5000



This document has been approved  
for public release and sale; its  
distribution is unlimited.

Prepared by

Jerome T. Chu  
Student

and

Sheng S. Li  
Professor

Department of Electrical Engineering  
University of Florida  
Gainesville, FL 32611

Tel. (904) 392-4937  
Fax (904) 392-8671  
E-mail: ShengLi@ENG.UFL.EDU

19950210 079

February 15, 1995

AASERT Grant #N00014-93-1-0827

**Third Semi-Annual Progress Report**  
(covering the period of 07/16/94-02/15/95)

**Project Title: Investigation of a Normal Incidence High-Performance P-type Strained Layer In<sub>0.3</sub>Ga<sub>0.7</sub>As/In<sub>0.52</sub>Al<sub>0.48</sub>As Quantum Well Infrared Photodetector.**

Submitted to

Max N. Yoder

Office of Naval Research  
Code 3140  
800 North Quincy Street  
Arlington, VA 22217-5000

Prepared by

Jerome T. Chu  
Student

and

Sheng S. Li  
Professor

Department of Electrical Engineering  
University of Florida  
Gainesville, FL 32611

Tel. (904) 392-4937  
Fax (904) 392-8671  
E-mail: ShengLi@ENG.UFL.EDU

Accession For	
NTIS	CRA&I
DTIC	TAB
Unannounced	
Justification	
By	
Distribution /	
Availability Codes	
Dist	Avail and/or Special
A-1	

February 15, 1995

REPORT DOCUMENTATION PAGE			Form Approved OMB No. 0704-0188
<p>Public reporting burden for this collection of information is estimated to average 1 hour per response, including the time for reviewing instructions, searching existing data sources, gathering and maintaining the data needed, and completing and reviewing the collection of information. Send comments regarding this burden estimate or any other aspect of this collection of information, including suggestions for reducing this burden, to Washington Headquarters Services, Directorate for Information Operations and Reports, 1215 Jefferson Davis Highway, Suite 1204, Arlington, VA 22202-4302, and to the Office of Management and Budget, Paperwork Reduction Project (0704-0188), Washington, DC 20503.</p>			
1. AGENCY USE ONLY (Leave blank)	2. REPORT DATE 15 Feb. 1995	3. REPORT TYPE AND DATES COVERED Progress Report: 07/16/94-02/15/95	
4. TITLE AND SUBTITLE Investigation of a Normal Incident High Performance P-type Strained Layer $In_{0.3}Ga_{0.7}As/In_{0.52}Ga_{0.48}As$ Quantum Well Infrared Photodetector		5. FUNDING NUMBERS ONR #N00014-93-1-0827	
6. AUTHOR(S) Jerome T. Chu, Student Sheng S. Li, Professor			
7. PERFORMING ORGANIZATION NAME(S) AND ADDRESS(ES)  University of Florida Gainesville, FL 32611-6200		8. PERFORMING ORGANIZATION REPORT NUMBER 92120712	
9. SPONSORING/MONITORING AGENCY NAME(S) AND ADDRESS(ES) US Navy, Office of Naval Research 800 North Quincy Street, Code 1512B:SM Arlington, VA 22217-5000		10. SPONSORING/MONITORING AGENCY REPORT NUMBER	
11. SUPPLEMENTARY NOTES			
12a. DISTRIBUTION/AVAILABILITY STATEMENT  Approved for public release, distribution unlimited.		12b. DISTRIBUTION CODE	
<p>13. ABSTRACT (Maximum 200 words)</p> <p>During this reporting period, we have made excellent progress towards the program goals. A significant achievement was made in the development of a new compressionally strained p-type GaAs/InGaAs QWIP grown on GaAs by MBE. This new QWIP achieved two color detection with detective peaks at 8.9 <math>\mu m</math> and 8.4 <math>\mu m</math> in the LWIR band and 5.5 <math>\mu m</math> in the MWIR band. This detector is under background limited performance (BLIP) at temperatures up to 70 K. The measured responsivity were found to be 24 mA/W and 45 mA/W for the two LWIR peaks respectively, while a responsivity of 13 mA/W was found for the MWIR peak; all at T=75 K. In addition, a new InGaAs/AlGaAs on GaAs compressionally strained p-QWIP was developed which exhibits extremely low dark currents and comparable responsivities when compared with the previous PCSL-QWIP. The measured responsivity was found to be 38 mA/W and 8mA/W at T=77 K, with the detective peaks at 7.4 and 5.5 <math>\mu m</math>, respectively. The detector is under BLIP conditions at T=63 K with applied biases from -3 V to +3 V.</p>			
14. SUBJECT TERMS P-type strained layer InGaAs/GaAs quantum well infrared photodetectors (QWIPs), intersubband absorption, dark current, responsivity, detectivity.		15. NUMBER OF PAGES	
		16. PRICE CODE	
17. SECURITY CLASSIFICATION OF REPORT Unclassified	18. SECURITY CLASSIFICATION OF THIS PAGE	19. SECURITY CLASSIFICATION OF ABSTRACT	20. LIMITATION OF ABSTRACT Unlimited

**Third Semi-Annual Progress Report (7/16/94-2/15/95)**

**Project Title: The Development of a Normal Incidence High Performance  
p-Type Strained Layer  $\text{In}_{0.3}\text{Ga}_{0.7}\text{As}/\text{In}_{0.52}\text{Al}_{0.48}\text{As}$  Quantum Well  
Infrared Photodetectors**

**Program Manager:** Max N. Yoder, Office of Naval Research, Code 3140, Arlington, VA.

**Principal Investigator:** Sheng S. Li, Professor, University of Florida, Gainesville, FL.

**Student :** Jerome T. Chu

**Project Objective:**

The objective of this project is to perform theoretical and experimental studies of dark current, photocurrent, optical absorption, spectral responsivity, noise, and detectivity for the normal incidence strained layer p-type III-V compound semiconductor quantum well infrared photodetectors (QWIPs) developed under this program. The material systems under investigation include InGaAs/InAlAs on InP substrates and GaAs/InGaAs or AlGaAs/InGaAs on GaAs substrates. The project will study the usage and effects of biaxial tension and compressional strain on the material systems and their effects towards photodetector design.

## I. Introduction

During the period of July 15, 1994 to February 15, 1995, significant progress has been made towards the design, fabrication, and characterization of strained layer p-type InGaAs/InAlAs on InP, GaAs/InGaAs on GaAs, and InGaAs/AlGaAs on GaAs quantum-well infrared photodetectors (P-QWIPs) in the 8-14  $\mu\text{m}$  range for staring focal plane arrays (FPAs). Specific tasks performed during this period include: (i) the continuing characterization and analysis of a normal incidence strained-layer p-type InGaA/GaAs QWIP on an GaAs substrate formed by molecular beam epitaxy (MBE) with a dual peak detective wavelength at 8.9  $\mu\text{m}$  and 8.4  $\mu\text{m}$  in the long wavelength infrared (LWIR) regime and a 5.5  $\mu\text{m}$  peak in the mid-wavelength infrared (MWIR) band, (ii) the design, growth, fabrication, and characterization of a normal incidence strained-layer p-type AlGaAs/InGaAs QWIP on a GaAs substrate with a peak long wavelength infrared (LWIR) detective wavelength at 7.5  $\mu\text{m}$  and a mid-wavelength infrared (MWIR) detective peak at 5.5  $\mu\text{m}$ , with extremely low dark currents. The following sections of this report will cover the technical results of the study during this reporting period and the research accomplishments and publications so far. A summary of the complete study is listed at the end of this report in table 1.

## II. Technical Results

### 2.1 Research Accomplishments and Publications

1. The design, growth, fabrication, and characterization of a compressively strained p-type InGaAs/GaAs QWIP on a GaAs substrate with peak wavelengths of  $\lambda_{p1} = 8.9 \mu\text{m}$  and  $\lambda_{p2} = 5.5 \mu\text{m}$ . Maximum responsivities of 93 mA/W and 30 mA/W were measured for each respective peak wavelength at 75 K. BLIP performance was achieved in the 8-14  $\mu\text{m}$  long wavelength infrared (LWIR) detection band at 70 K and under 0.3 V of applied bias.
2. The design, growth, fabrication, and characterization of a dual strain InGaAs/AlGaAs P-QWIP on a GaAs substrate with a peak wavelength of 7.5  $\mu\text{m}$  and a mid-wavelength infrared (MWIR) peak at 5.5  $\mu\text{m}$ . Very low dark current densities for this device were

measured at 77 K. Maximum responsivities of 40 mA/W and 8 mA/W were measured for each respective wavelengths at 77 K under an applied bias of +5.0 V with operation at up to 85 K possible under moderate bias ( $\leq 2$  V) BLIP performance was achieved both detection bands at 63 K within the applied bias range of -2.7 V to 3.0 V.

**A. Journal Papers:**

1. Y. H. Wang, S. S. Li, and J. Chu and Pin Ho, "An Ultra-low Dark Current P-type Strained-layer InGaAs/InAlAs Quantum Well Infrared Photodetector with Background Limited Performance (BLIP)" *Appl. Phys. Letts*, Feb. 7 issue, 1994.
2. Y. H. Wang, S. S. Li, and J. Chu and Pin Ho, "A Normal Incidence P-type Compressive Strained-Layer InGaAs/GaAs Quantum Well Infrared Photodetector for Mid-Wavelength Infrared (MWIR) and Long-Wavelength Infrared (LWIR) Detection" *J. Appl. Phys.*, accepted, July 1994.

**B. Conference Presentations:**

1. S. S. Li, J. Chu, and Y. H. Wang, "A Normal Incidence P-type Strained Layer InGaAs/InAlAs Quantum Well Infrared Photodetector with Background Limited Performance at 77 K", presented at the 1994 SPIE symposium, Orlando, FL, April 4-8, 1994.
2. Pin Ho, Y. H. Wang, S. S. Li, and J. Chu, "MBE Growth of P-type Strained-layer InGaAs/InAlAs QWIPs", presented at the 1994 14th North American Conference on Molecular-beam Epitaxy, Urbana-Champaign, IL, October 10-12, 1994.
3. Y. H. Wang, J. Chu, S. S. Li, and Pin Ho, "A Normal Incidence P-type Compressive Strained-Layer InGaAs/GaAs Quantum Well Infrared Photodetector", 2nd. International Conference on 2-20  $\mu$ m Wavelength Infrared Detectors and Arrays, Miami Beach, FL, October 9-14, 1994.
4. S. S. Li, Y. H. Wang, and J. Chu, "A New Class of Normal Incidence Strained-Layer III-V Quantum Well Infrared Photodetectors", presented at the 1994 LEOS Conference, Boston, MA, October 31-November 3, 1994.

## 2.2 P-QWIP Operation and Design Theory

With the advent of advanced molecular beam epitaxial technologies in the last few decades, device structures utilizing heterostructure quantum wells have been heavily explored. N-type quantum well infrared photodetectors (QWIPs) have been extensively studied in the recent years<sup>1-2,28</sup>. These systems use GaAs/AlGaAs and InGaAs/InAlAs structures for detection in the 3 - 5  $\mu\text{m}$  mid-wavelength infrared (MWIR) and 8 - 14  $\mu\text{m}$  LWIR atmospheric transmission windows. Since n-type GaAs/InGaAs and InGaAs/InAlAs QWIPs have inherently low electron effective masses and high electron mobilities, they offer excellent infrared (IR) detection properties. Due to the quantum mechanical selection rules which prohibit normal incidence intersubband absorption, focal plane arrays (FPA) using n-type QWIPs must use either metal or dielectric gratings to couple normal incidence IR radiation into the quantum well<sup>2-4</sup>. In contrast, because of the mixing between the light hole and heavy hole states under either biaxial tension or compressional strain, normal incidence illumination is allowed for the intersubband transition in p-type QWIPs; thus eliminating the need for metal or dielectric grating couplers.

### 2.2.1 P-QWIP Physics

#### 2.2.1.1 Strained Layer Growth Limitations and Theory

P-type QWIPs using valence intersubband transitions have been demonstrated<sup>5-7</sup> in lattice-matched GaAs/AlGaAs and InGaAs/InAlAs material systems. In general, intersubband transitions excited by normal incidence radiation in p-type quantum wells are allowed since a linear combination of p-like valence band Bloch states exists, which provides a nonzero coupling between the normal radiation field and valence band Bloch states. The strong mixing between the heavy hole and the light hole states greatly enhances intersubband absorption. The drawback of using lattice-matched systems is the fact that the intersubband transition occurs between the heavy hole ground states and the upper excited states. Because of the relatively large heavy hole effective mass when compared to the electron effective mass, relatively weak absorption and therefore similarly low responsivity is predicted in the

IR wavelength range when compared to n-type QWIPs. In order to increase the absorption characteristics and responsivity of P-QWIPs, biaxial stress is introduced into the well layers of the QWIP structure. If the intentionally introduced biaxial stress between the well layers and the barrier layers contained in the layer thickness (the total thickness of the wells and barriers) in the P-QWIP structure is less than the critical thickness, then pseudomorphic or coherent heterointerfaces can be grown without the introduction of defects between the layers. Based upon the force balance model<sup>8,29-30</sup>, the equilibrium critical layer thickness,  $L_c$ , for an epilayer with the lattice constant,  $a$ , grown on a substrate with a lattice constant,  $a_s$ , is given as

$$L_c = \left( \frac{a}{\sqrt{2}\delta_o} \right) \frac{1 - \nu \cos^2 \Theta}{8\pi(1 + \nu) \cos \alpha} \left[ 1 + \ln(h\sqrt{2}/a) \right], \quad (1)$$

where  $h$  is the epilayer thickness,  $\Theta$  is the angle between the dislocation line and the Burges' vector,  $\alpha$  is the angle between the slip direction and the layer plane direction,  $\delta_o$  is the lattice-mismatch or the in-plane strain, and  $\nu$  is the Poisson ratio.  $\delta_o$  is defined as  $\delta_o = (a_s - a)/a$  where  $\delta_o > 0$  for tensile strain and  $\delta_o < 0$  for compressive strain. Similarly,  $\nu$  is defined as  $\nu = -C_{12}/C_{11}$ .  $C_{ij}$ 's are the elastic constants and can be found in reference 9.

The strained-layers have the same effective in-plane lattice constant,  $a_{\parallel}$  (i.e.,  $a_{x,y}$ ), and can store the excess energy due to the elastic strain within the layers. The in-plane lattice constant,  $a_{\parallel}$ , can be expressed by<sup>8</sup>

$$a_{\parallel} = a_1 \left[ 1 + \delta_o / \left( 1 + \frac{\xi_1 L_1}{\xi_2 L_2} \right) \right], \quad (2)$$

where  $a_{1,2}$  and  $L_{1,2}$  are the individual layer lattice constants and thicknesses, respectively, and  $\xi_{1,2}$  are the shear moduli as described by  $\xi = (C_{11} + C_{12} - 2C_{12}^2/C_{11})$ , where the  $C_{ij}$ 's are elastic constants for the strained material.  $\delta_o$  denotes the lattice mismatch between layers and  $a_{1,2}$  are the lattice constants of the strained well and the substrate (or barrier) respectively. When  $a_{\parallel} \neq a_s$ , the coherently strained superlattice structure is no longer in equilibrium with the substrate. If the lattice constant of the barrier layers is equal to that of the substrate, the the strain will be completely accomodated in the well layers with no strain in the barrier layers. However, Hull et al.<sup>22</sup> showed that if the individual layers thicknesses in the superlattice is less than its critical thickness, even though  $a_{\parallel} \neq a_s$ , the loss of coherence only occurs at the interface between the whole superlattice and the substrate, while the

superlattice itself remains coherent.

### 2.2.1.2 Strain Induced Energy Band Shifts

If the QWIP structure is grown along the [100] direction and the strained-layer is within the critical thickness,  $L_c$ , then a pseudomorphic or coherent heterointerface can be obtained and the components of the strain tensor  $[e]$  are simplified to the expressions given by

$$e_{xx} = e_{yy} = e_{\parallel} \quad (3)$$

$$e_{zz} = -e_{\parallel} \left( \frac{2C_{12}}{C_{11}} \right) \quad (4)$$

$$e_{xy} = e_{yz} = e_{zx} = 0. \quad (5)$$

In addition to altering the physical parameters of the QWIP, lattice strain can also induce energy band shifts, which can be used to alter the absorption characteristics of the QWIP. The strain induced energy band shifts for the conduction band, the heavy hole subband, and light hole subband can be approximated as follows.

$$\Delta E_c = 2c_1 \frac{C_{11} - C_{12}}{C_{11}} \delta_o \quad (6)$$

$$\Delta E_{hh} = b \frac{C_{11} + C_{12}}{C_{11}} \delta_o \quad (7)$$

$$\Delta E_{lh} = -\Delta E_{hh} + \frac{(\Delta E_{hh})^2}{2\Delta_o} \quad (8)$$

where  $c_1$  is the combined hydrostatic deformation potential which characterizes the splitting of the  $\Gamma_8$  valence band under strain and  $b$  is the shear deformation potential and  $\Delta_o$  is the spin orbit split-off energy<sup>9</sup>. The total hydrostatic deformation potential ( $c_1 + V_v$ ), where  $V_v$  is the valence band deformation potential, can be expressed by<sup>10</sup>

$$c_1 + V_v = -\frac{1}{3}(C_{11} + 2C_{12}) \frac{dE_g^o}{dP}, \quad (9)$$

where  $dE_g^o/dP$  is the unstrained energy bandgap change with respect to the unit pressure.

The effect of strain on the energy band structure results in the splitting of the heavy hole and light hole band at the valence band zone center<sup>11</sup> (i.e., the in-plane wavevector  $k_{\parallel} = 0$ ), which is degenerate in the unstrained case. When tensile strain is applied between the quantum well and the barrier layers<sup>12-14</sup> along the superlattice growth z-direction, the strain can push the light hole levels upwards and pull the heavy hole levels downwards. We

can therefore expect that heavy hole and light hole states can be inverted at specific lattice strains and quantum well thicknesses. This phenomena will in turn cause the intersubband transitions in a QWIP structure to take place from the populated light hole ground state to the upper energy band states. Since the light hole has a small effective mass (comparable to the electron effective mass), the optical absorption and photon responsivity in p-type QWIPs can be greatly enhanced, as a result of introducing strain in the quantum well. In addition to the utilization of the light hole states for their small effective masses, etc., certain heavy hole states under compressional strain may also have similar characteristics, like high mobilities, small effective masses, and long mean free paths; which in turn favorably alter the intersubband absorbtion and transport characteristics, as shown by Hirose, et al.<sup>31</sup>. This is achieved by distorting the heavy hole valence band at and near the zone center via the introduction of compressional strain.

### 2.2.1.3 Energy Band Calculations

To calculate the locations of the energy subbands, we can use the transfer matrix method (TMM)<sup>13,15</sup>, based on the eight-band  $\mathbf{k} \cdot \mathbf{p}$  model. This model is represented by the Luttinger-Kohn Hamiltonian<sup>16-17</sup>,  $H_t$ , which describes the unstrained semiconductor.

$$H_t = H + V(z) \quad (10)$$

where

$$H = \begin{bmatrix} H_{11} & H_{12} & H_{13} & H_{14} \\ H_{21} & H_{22} & H_{23} & H_{24} \\ H_{31} & H_{32} & H_{33} & H_{34} \\ H_{41} & H_{42} & H_{43} & H_{44} \end{bmatrix} \quad (11)$$

with:

$$\begin{aligned} H_{11} &= \frac{\gamma_1 + \gamma_2}{2} (k_x^2 + k_y^2) + \frac{\gamma_1 - \gamma_2}{2} k_z^2 \\ H_{22} &= \frac{\gamma_1 - \gamma_2}{2} (k_x^2 + K_y^2) + \frac{\gamma_1 + \gamma_2}{2} k_z^2 \\ H_{12} &= i\sqrt{3}\gamma_3(k_x - ik_y)k_z \\ H_{13} &= \frac{\gamma_2\sqrt{3}}{2}(k_x^2 - k_y^2) - i\sqrt{3}\gamma_3 k_x k_y \\ H_{21} &= H_{12}^* & H_{13} &= H_{31}^* & H_{24} &= H_{13} \\ H_{34} &= H_{12} & H_{42}^* &= H_{13}^* & H_{43} &= H_{12}^* \end{aligned}$$

$$H_{14} = H_{23} = H_{32} = H_{41} = 0$$

and  $V(z)$  is a step function where  $V(z)$  vanishes inside the well layers and equals  $V_o$  in the barrier layers. The effect of strain is included by adding the Pikus-Bir Hamiltonian<sup>18</sup>,  $H_s$ , to the general Luttinger-Kohn Hamiltonian. As shown below, the strain Hamiltonian for the well material is a diagonal matrix.

$$H_s = \begin{bmatrix} -\Delta E_c - \Delta E_{hh} & 0 & 0 & 0 \\ 0 & -\Delta E_c + \Delta E_{hh} & 0 & 0 \\ 0 & 0 & -\Delta E_c + \Delta E_{hh} & 0 \\ 0 & 0 & 0 & \Delta E_c + \Delta E_{hh} \end{bmatrix} \quad (12)$$

Using the aforementioned techniques, we can numerically calculate the energy of the zone-center valence subband levels as a function of well width for any material system under tensile or compressional strain and also determine the change in the valence subband structures.

All of the previously described calculations are derived from the multiband effective mass  $\mathbf{k} \cdot \mathbf{p}$  model for a coherently strained structure, which is based upon the perturbation approximation. In the  $\mathbf{k} \cdot \mathbf{p}$  model, the interactions of S-P type coupling among conduction (C), light-hole (LH), heavy-hole (HH), and spin-orbit (SO) states combined with spin-orbit like coupling are taking into consideration to derive the band structures. This results in an  $8 \times 8 \mathbf{k} \cdot \mathbf{p}$  Hamiltonian and momentum matrix elements. Using the perturbation approximation, a set of wave functions of  $S_{1/2}$ :  $|1/2, \pm 1/2\rangle_c$ ;  $P_{3/2}$ :  $|3/2, \pm 3/2\rangle$ ,  $|3/2, \pm 1/2\rangle$ ; and  $P_{1/2}$ :  $|1/2, \pm 1/2\rangle$  are used to represent the unperturbed and unstrained basis in the  $|J, m_j\rangle$  presentation<sup>23</sup>.  $m_j = \pm 1/2$  represents either the electron or LH states, while  $m_j = \pm 3/2$  denotes the HH or heavy particle states. A slightly simplified  $6 \times 6 \mathbf{k} \cdot \mathbf{p}$  Hamiltonian can be used to roughly predict the P-like properties of the coherently strained layers by considering the S-like conduction band states as a perturbation, if a large enough bandgap exists, like in InGaAs and GaAs layers. The wave functions of the coherently strained superlattice at the zone center ( $\mathbf{k}=0$ ) are given by<sup>24</sup>

$$|3/2, \pm 3/2\rangle \quad HH\text{ states} \quad (13)$$

$$\gamma|3/2, \pm 1/2\rangle + \beta|1/2, \pm 1/2\rangle \quad LH\text{ states} \quad (14)$$

$$-\beta|3/2, \pm 1/2\rangle + \gamma|1/2, \pm 1/2\rangle \quad SO\text{ states} \quad (15)$$

where  $\gamma$  and  $\beta$  are constants which are dependent on the strain parameters. Note that the heavy-hole states,  $|3/2, \pm 3/2\rangle$ , are still decoupled from the other valence band states even under biaxial stress at the zone center, while the light-hole and spin-orbit split off states are coupled at  $\mathbf{k}=0$ . However, the HH, LH, and SO states are mixed<sup>25,26</sup> in the coherently strained superlattice at off zone center ( $\mathbf{k}\neq 0$ ). This mixing between the states with different  $m_j$ 's is due to the boundary conditions across the interface of the quantum well layers. By examining the  $\mathbf{k} \cdot \mathbf{p}$  matrix, we can see that the interaction between the different  $m_j$  states is proportional to the transverse components of the wave vector,  $\mathbf{k}_{x,y}$ , so that the HH states are decoupled when  $\mathbf{k}_{x,y}=0$ . It is interesting to note that the  $\mathbf{k}_{x,y}$ 's are conserved across the interfaces since the interface potential depends only on  $z$ , the quantum well growth direction. Thus the band mixing can be significant if the  $\Gamma$ -bandgap is small, like with GaAs and InGaAs, and if the LH and SO bands involved in the transition have a large  $k_z$  value<sup>25</sup>.

Since the heavy hole and light hole valence subbands are non-degenerate following the introduction of strain into the QWIP structure, a simpler method can be used to determine the energies of the subbands. By using the parabolic band approximation near the valence band zone-center, and the energy band shifts for the conduction band minimum, heavy hole subband maximum, and light hole subband maximum, we can utilize the simpler two-band Hamiltonian for electrons just by finding the effective mass of the carriers (i.e., heavy hole effective mass and light hole effective mass) and the barrier heights for each carrier type. Although this does not simultaneously determine the energy levels of both carriers, it does allow accurate predictions of the energy subbands. When compared to the direct calculation of the energy subbands, the two-band approximation yields accurate results when compared to the direct calculation results<sup>13,18</sup> (see also figures 1(a)-1(c)). One limitation of the TMM is that this method cannot calculate the energy levels of the allowed energy subbands in the continuum states. In order to determine the transition energy from the ground state to the continuous state, we used the Kronig-Penney model to determine the locations of the allowed energy bands in the continuum states.

As can be seen in figures 1(b) and 1(c), the influence of strain on the relative positions of the heavy hole (HH) and light hole (LH) subbands is apparent. When a biaxial internal tension is applied to the well material (in this case  $\text{Ga}_{0.7}\text{In}_{0.3}\text{As}$  on an InP substrate with the barrier layers consisting of lattice matched  $\text{Al}_{0.48}\text{In}_{0.52}\text{As}$ ), the strain pulls the LH subbands

up with respect to the HH subbands for a given well thickness. While quantum confinement effects tend to push the LH subbands down with respect to the HH subbands. As the well width is increased above a certain value, the strain effect can overcome the quantum confinement effect and therefore induce the inversion of the heavy hole and light hole subbands at the ground state. In contrast, with the application of compressional strain on the well layers, as we see in the  $\text{In}_{0.4}\text{Ga}_{0.6}\text{As}/\text{GaAs}$  quantum well structure, the strain pushes the LH subbands down with respect to the HH subbands for a given well thickness.

#### 2.2.1.4 The Transfer Matrix Method for the Calculation of Transmission Probability

The transfer matrix method (TMM)<sup>33</sup> allows the calculation of the transmission probability through a superlattice. Like any typical quantum mechanical barrier or well, the carrier conduction in each layer of the superlattice consists of the superposition of two components propagating forwards and backwards. The complete wave function can be expressed as

$$\psi_i = \psi_i^+ e^{+ik_i} e^{-\Delta_i} + \psi_i^- e^{-k_i} e^{+\Delta_i} \quad (16)$$

where

$$\begin{aligned} \Delta_1 &= \Delta_2 = 0 \\ \Delta_i &= k_i(d_2 + d_3 + \dots + d_i) \\ i &= 3, 4, \dots, N \\ k_i &= \left[ \frac{2m_i^*}{\hbar^2} (E - E_i) \right]^{1/2}, \end{aligned}$$

where  $\psi_i^+$  and  $\psi_i^-$  represent the magnitudes of the wave functions propagating in the forward, or  $+z$  direction and the backwards, or  $-z$  direction, respectively. While  $N$  is the number of periods in the superlattice,  $d_i$  is the thickness of the  $i$ -th layer in the superlattice,  $m_i^*$  is the effective mass of the particle in the  $i$ -th superlattice layer, and  $E_i$  is the potential energy of the  $i$ -th layer. Since the wave function,  $\psi$ , and its derivative,  $d\psi/dz$ , are continuous at the boundaries, the wave functions then become

$$\psi_i^+ = (e^{-i\delta_i} \psi_{i+1}^+ + r_i e^{-i\delta_i} \psi_{i+1}^-) / t_i \quad (17)$$

$$\psi_i^- = (r_i e^{i\delta_i} \psi_{i+1}^+ + e^{i\delta_i} \psi_{i+1}^-) / t_i. \quad (18)$$

The recurrence relationship of the wave functions can be written in matrix form as

$$\begin{pmatrix} \psi_i^+ \\ \psi_i^- \end{pmatrix} = \frac{1}{t_i} \begin{pmatrix} e^{-i\delta_i} & r_i e^{-i\delta_i} \\ r_i e^{i\delta_i} & e^{i\delta_i} \end{pmatrix} \begin{pmatrix} \psi_{i+1}^+ \\ \psi_{i+1}^- \end{pmatrix}, \quad (19)$$

where at normal incidence

$$r_i = \frac{k_i - k_{i+1}}{k_i + k_{i+1}}, \quad (20)$$

$$t_i = \frac{2k_i}{k_i + k_{i+1}}, \quad (21)$$

and

$$\delta_i = k_i d_i. \quad (22)$$

Which gives us the following form for determining the  $N + 1$ -th wave functions

$$\begin{pmatrix} \psi_1^+ \\ \psi_1^- \end{pmatrix} = S_1 \begin{pmatrix} \psi_2^+ \\ \psi_2^- \end{pmatrix} = S_1 S_2 \begin{pmatrix} \psi_3^+ \\ \psi_3^- \end{pmatrix} = S_1 S_2 \cdots S_N \begin{pmatrix} \psi_{N+1}^+ \\ \psi_{N+1}^- \end{pmatrix}, \quad (23)$$

given that

$$S_i = \frac{1}{t_i} \begin{pmatrix} e^{-i\delta_i} & r_i e^{-i\delta_i} \\ r_i e^{i\delta_i} & e^{i\delta_i} \end{pmatrix}. \quad (24)$$

Since there is no backwards, or in the  $-z$  direction, propagation in the  $N + 1$ -th layer, the magnitude of the wave function  $\psi_{N+1}^- = 0$ . Then we can find the  $\psi_i^+$  term of  $E_1^+$ , in the  $i$ -th layer ( $i = 2, 3, 4, \dots, N + 1$ ).

If we determine the quantity,  $\psi_i^+/\psi_1^+$ , as a function of  $E_1$ , then we will know the locations of the resonant peaks. The transmission probability can then be given as

$$|T \cdot T| = \left| \frac{\psi_i^+}{\psi_1^+} \right|^2. \quad (25)$$

### 2.2.1.5 Determination of Intersubband Transitions and Absorption Coefficients

In addition to the energy level and energy band locations, the calculation of intersubband and interband transitions are also of great interest. In order to determine the intersubband and interband transitions in a p-type strained layer QWIP, the usage of the  $6 \times 6$  Hamiltonian which includes the previously mentioned  $\mathbf{k} \cdot \mathbf{p}$  Hamiltonian<sup>16-17,24</sup> and the

strain Hamiltonian<sup>18</sup>. Since the strain and the pin-orbit coupling terms do not lift the spin degeneracy, the  $6 \times 6$  Hamiltonian matrix can then be factorized into two  $3 \times 3$  irreducible matrices. The assumption that the Fermi distribution function is equal to one for the confined ground state and is equal to zero for the excited states in equilibrium is used to simplify the calculation without loss of accuracy. The absorption coefficient for the intersubband or interband transition between the initial ground state,  $i$ , and the final continuum state,  $f$ , is given by<sup>27</sup>

$$\alpha_i(\omega) = \sum_f \frac{4\pi^2 e^2}{n_r c m_o^2 \omega} \int_{BZ} \frac{2d\mathbf{k}}{(2\pi)^3} \left[ (f_i - f_f) |\hat{\epsilon} \cdot \mathbf{P}_{i,f}|^2 \frac{\Gamma/2\pi}{[\Delta_{i,f}(\mathbf{k}) - \hbar\omega]^2 + (\Gamma^2/4)} \right] \quad (26)$$

where  $n_r$  is the refractive index in the quantum well,  $m_o$  is the free electron mass,  $\Delta_{i,f}$  is the energy difference between the initial ground state,  $i$ , of energy  $E_i(\mathbf{k})$  and the final state,  $f$ , with the corresponding energy of  $E_f(\mathbf{k})$ .  $\hat{\epsilon}$  and  $\omega$  are the unit polarization vector and the frequency of the incident IR radiation, respectively,  $f_i$  and  $f_f$  are the Fermi distribution functions of the initial and final states, and  $\Gamma$  is the full width of level broadening.  $\Gamma \sim \hbar/\tau_{if}$ , where  $\tau_{if}$  is the lifetime between the initial,  $i$ , and final,  $f$ , states.  $|\hat{\epsilon} \cdot \mathbf{P}_{i,f}|$  are the optical transition elements between the quantum well valence subband ground states,  $i$ , and the continuum subband states,  $f$ , in the HH, LH, and SO bands; which can be derived from the two  $3 \times 3 \mathbf{k} \cdot \mathbf{p}$  matrix elements as shown below.

Using the following  $3 \times 3$  optical matrix,

$$\frac{m_o}{\hbar} \begin{bmatrix} T_{HH} & T_{HL} & T_{HS} \\ T_{LH} & T_{LL} & T_{LS} \\ T_{SH} & T_{SL} & T_{SS} \end{bmatrix}, \quad (27)$$

the optical matrix elements,  $|\hat{\epsilon} \cdot \mathbf{P}_{i,f}|$ , can be obtained. These matrix elements have the same form as the  $\mathbf{k} \cdot \mathbf{p}$  matrix elements except that the  $k_i k_j$ 's are replaced with  $k_i \epsilon_j + k_j \epsilon_i$  multiplied by a constant factor of  $m_o/\hbar$ .<sup>27</sup> The  $T_{ij}$ 's are defined as follows:

$$T_{HH} = 2(A - B)\epsilon_z k_z + (2A + B)(\epsilon_x k_x + \epsilon_y k_y), \quad (28)$$

$$T_{LL} = 2(A + B)\epsilon_z k_z + (2A - B)(\epsilon_x k_x + \epsilon_y k_y), \quad (29)$$

$$T_{SS} = 2A(\epsilon_x k_x + \epsilon_y k_y + \epsilon_z k_z) \quad (30)$$

$$T_{HL} = i \frac{1}{\sqrt{3}} N (\epsilon_x \cos \eta - \epsilon_y \sin \eta) k_z - i \frac{1}{3} N \epsilon_z k_{||}$$

$$\begin{aligned}
& -\sqrt{3}B(\epsilon_x k_x - \epsilon_y k_y) \cos \chi \\
& + \frac{1}{\sqrt{3}}N(\epsilon_x k_y + \epsilon_y k_x) \sin \chi,
\end{aligned} \tag{31}$$

$$\begin{aligned}
T_{HS} = & \frac{1}{\sqrt{6}}N(\epsilon_x \cos \eta + \epsilon_y \sin \eta)k_z + \frac{1}{6}N\epsilon_z k_{\parallel} \\
& + i\sqrt{6}B(\epsilon_x k_x - \epsilon_y k_y) \cos \chi \\
& - \frac{2}{\sqrt{6}}N(\epsilon_x k_y + \epsilon_y k_x) \sin \chi,
\end{aligned} \tag{32}$$

$$\begin{aligned}
T_{LS} = & \left[ i2\sqrt{2}B\epsilon_z + \frac{1}{\sqrt{2}}N\epsilon_x \cos(\chi - \eta) - \epsilon_y \sin(\chi - \eta) \right] k_z \\
& - i\sqrt{2}B(\epsilon_x k_x + \epsilon_y k_y) \\
& - \frac{1}{\sqrt{2}}N\epsilon_z k_{\parallel} \cos(\chi - 2\eta),
\end{aligned} \tag{33}$$

$$T_{SH} = T_{HS}^*, \tag{34}$$

$$T_{SL} = T_{LS}^*, \tag{35}$$

$$T_{LH}^* = T_{HL}^*. \tag{36}$$

Here  $A, B, N, \chi, \eta$  are inverse mass band parameters.<sup>27</sup>

#### 2.2.1.6 Photoconductive Detection Mode Operation

Most QWIPs reported in the literature are operated in the photoconductive (PC) mode, which is dependent on an externally applied bias. So far, the p-QWIPs which we have studied have all been operated in the PC mode.

When IR radiation is incident on a photoconductor it exhibits a change in resistance,  $\Delta R_d$ . This change in resistance is due to the photo-excitation of carriers, forming mobile excess carriers in the photoconductor. The photogenerated carriers,  $\Delta n$ , can be expressed as

$$\Delta n = \frac{\eta \Delta \Phi \tau_L}{V_d} \tag{37}$$

where,  $\eta$ , is the quantum efficiency,  $\Delta \Phi$  is the incident photon flux,  $\tau_L$  is the excess carrier lifetime, and  $V_d$  is the volume of the detector. These photogenerated carriers are transported out of the detector under the influence of the applied external bias, which results in a photovoltage signal. The change in the output photovoltage,  $\Delta V_o$ , due to the resistance change is given by

$$\Delta V_o = -\frac{V_a R_L \Delta R_d}{(R_L + R_d)^2}, \tag{38}$$

where  $R_L$  is the load resistance and its value is chosen to be about equal to  $R_d$ , the detector resistance, to match loads and optimize the output signal.

### 2.2.2 P-QWIP Figures of Merit

Although our band structure and absorption calculations can be used to determine the positions of the subbands in the quantum wells, and hence determine the peak absorption wavelength of the QWIP, many other factors must be taken into account to create a successful detector. Generally, for a useful detector, the responsivity must be high, while the noise current, and therefore dark current, must be low.

#### 2.2.2.1 Spectral Responsivity

The responsivity,  $R$ , for a photodetector may be expressed as<sup>19</sup>

$$R = \frac{q\lambda\eta}{hc} G = \frac{q}{h\nu} \eta_c, \quad (39)$$

where  $q$  is the electronic charge,  $\lambda$  is the wavelength of the incident photon,  $h$  is the Planck constant,  $c$  is the speed of light,  $\eta$  is the quantum efficiency,  $\eta_c$  is the collection efficiency,  $\nu$  is the incident frequency, and the photoconductive gain is  $G$ . The quantum efficiency and photoconductive gain are described, respectively, by<sup>19</sup>

$$\eta = A(1 - R)[1 - \exp(-B\alpha l_{qw})] \quad (40)$$

$$G = \frac{L}{t_c} \quad (41)$$

where  $A$  is a constant that is polarization dependent,  $\alpha$  is the absorption coefficient of the quantum well,  $l_{qw}$  is the total width of all quantum well regions,  $L$  is the mean free path of the carrier,  $R$  is the reflection coefficient, and  $t_c$  is the total width of all quantum well and barrier regions.  $B$  is a constant dependent on the number of passes IR radiation makes through the photodetector. For n-type QWIPs,  $A=0.5$ , while for p-type QWIPs  $A=1$ . The mean free path of the carrier may be expressed as<sup>19</sup>

$$L = \tau T_{qw} \mu_{eff} E, \quad (42)$$

where  $\tau$  is the well recapture lifetime of the carrier,  $T_{qw}$  is the transmission coefficient over the quantum well,  $\mu_{eff}$  is the effective mobility of the carrier, and  $E$  is the electric field. The

effective mobility for a two-band transport model is shown to be<sup>19</sup>

$$\mu_{eff} = \frac{\Delta p_{lh}\mu_{lh} + \Delta p_{hh}\mu_{hh}}{\Delta p_{lh} + \Delta p_{hh}}, \quad (43)$$

where  $\Delta p_{hh}$  and  $\Delta p_{lh}$  are the concentrations of optically induced heavy and light hole carriers respectively, and  $\mu_{hh}$  and  $\mu_{lh}$  are the respective heavy and light hole mobilities. When only the ground state is completely occupied, either  $\Delta p_{lh}$  or  $\Delta p_{hh}$ , the optically induced light holes or the optically induced heavy holes dominate, so that we may estimate  $\mu_{eff}$  as the in-plane effective mass of the ground state carriers.

### 2.2.2.2 QWIP Collection Efficiency

A figure of merit that is easily quantified by simple measurements is the collection efficiency,  $\eta_c$ . The collection efficiency describes the ease in which the energy from the incident photon flux is converted into mobile carriers which are swept out of the QWIP and collected; and is defined as the product of the quantum efficiency,  $\nu$ , and the photoconductive gain,  $G$ .

$$\eta_c = \eta G \quad (44)$$

In addition to being expressed as the mean free path over the total width of the quantum wells and barriers,  $G$  can be viewed as the ratio of the carrier transport lifetime,  $\tau_L$ , to the transit time,  $\tau_T$ , through the QWIP. Empirically, the photoconductive gain can be described in terms of the capture or trapping probability,  $p_c$ ,<sup>34-36</sup>

$$G = \frac{1 - p_c}{N p_c}, \quad (45)$$

and  $N$  is the free carrier density.

Physically, the trapping probability is defined as the ratio of the escape time from the well region to the lifetime of the excited carriers from the confined ground state. If the excited states are in resonance with the top of the barrier potential energy, then the escape time will be greatly reduced, which minimizes the trapping probability and maximizes the photoconductive gain.

An approximate expression for  $\nu_c$  can be expressed as follows with the caveat that the expression only works if  $B\alpha l_{qw} \ll 1$  and  $p_c \ll 1$ .

$$\eta_c = A(1 - R)[1 - \exp(-B\alpha l_{qw})] \frac{1 - p_c}{N p_c} \quad (46)$$

$$\approx A(1-R) \frac{B\alpha l_{qw}}{Np_c}. \quad (47)$$

### 2.2.2.3 Dark Current Relationships in QWIPs

Another important parameter to be considered in a QWIP design is the dark current density ( $J_d$ ), which is expressed using the Richardson-Dushman equation<sup>14</sup> as

$$J_d \propto T^2 m^* \exp\left(\frac{-\Delta E}{kT}\right), \quad (48)$$

where  $m^*$  is the effective mass,  $\Delta E$  is the difference in energy between the barrier height and the quantum confined state in the well,  $k$  is the Boltzmann constant, and  $T$  is the temperature. This type of expression assumes that the dominant source of dark current is thermionic emission over the quantum well barrier.

In the low-field regime, the thermionic emission current is related to the density of mobile carriers,  $n_t$  and the average drift velocity,  $v_d$ . It can be expressed as<sup>37</sup>

$$I_{th} = eA_d v_d n_t, \quad (49)$$

where  $A_d$  is the active detector area,  $e$  is the electronic charge, and

$$v_d = \frac{\mu \varepsilon}{[1 + (\mu \varepsilon / v_s)^2]^{1/2}}, \quad (50)$$

$$n_t = (m^* k_b T / \pi \hbar^2 L) \exp[-(E_{cf} - E_F) / k_b T]. \quad (51)$$

In these relationships,  $\mu$  is the mobility,  $\varepsilon$  is the electric field,  $v_s$  is the saturation velocity,  $E_{cf}$  is the cut-off energy related to the cut-off wavelength  $\lambda_c$ , and  $m^*/\pi \hbar^2$  is the two-dimensional density of states. The Fermi energy,  $E_F$ , can be obtained as

$$N_D = \frac{m^* k_b T}{\pi \hbar^2 L} \sum_n \ln \left[ 1 + \exp\left(\frac{E_F - E_n}{k_b T}\right) \right] \quad (52)$$

$$\approx \frac{m^*}{\pi \hbar^2 L} \sum_n (E_F - E_n), \quad (53)$$

with the understanding that the exact expression for  $N_D$  is valid when summed over the subband levels  $E_n$  below the Fermi level, and the approximate expression is only valid at cryogenic temperatures.

Using the previous result in the cryogenic temperature range, we see that the dark current due to thermionic emission is exponentially proportional to the doping concentration in the quantum well, as expressed below,

$$I_{th} \propto \exp \frac{E_F}{k_B T} \propto \exp \frac{N_D}{k_B T}. \quad (54)$$

So as the doping density in the quantum well increases, the dark current density due to thermionic emission increases exponentially. In contrast to this, the intersubband absorption is directly proportional to the doping concentration. Therefore, a tradeoff between dark current density and intersubband absorption is required to optimize QWIP performance.

#### 2.2.2.4 Noise in QWIPs

The noise in QWIP structures is mainly due to random fluctuations of thermally excited carriers. The noise is expressed as<sup>5</sup>

$$i_{noise} = \sqrt{4A_d q G \Delta f J_d}, \quad (55)$$

where  $A_d$  is the detector area, and  $\Delta f$  is the bandwidth. Finally, a figure of merit measurement used to compare detectors is the detectivity,  $D^*$ , which is shown to be<sup>19</sup>

$$D^* = \sqrt{A_d \Delta f} \frac{R}{i_{noise}}. \quad (56)$$

If the dark current in a particular QWIP is lower than the 300 K background photocurrent, then the QWIP can be considered to be under background limited performance (BLIP). In a BLIP limited QWIP, the dominant current is due to photon noise, since all the other sources are negligible by comparison. The photon noise is calculated from the arrival statistics of the incoherent photons. The background photon noise current,  $i_{np}$ , is given by<sup>20,21</sup>

$$i_{np}^2 = 4Aq^2 \eta g^2 P_b B / (h\nu), \quad (57)$$

where  $P_b$  is the incident background optical power,  $B$  is the QWIP bandwidth,  $\eta$  is the absorption quantum efficiency,  $\nu$  is the incident photon frequency, and  $g$  is the photoconductive gain. The photocurrent,  $I_p$  can be approximated by

$$I_p = A(q/h\nu) \eta g P_s, \quad (58)$$

where  $P_s$  is the incident optical signal power. The constant,  $A$ , in Eqs. (46), (47), (57), and (58), is due to the polarization selectivity for n-type QWIPs versus p-type QWIPs. As previously stated, for n-type QWIPs,  $A = 0.5$ , while  $A = 1$  for p-type QWIPs. By setting the signal-to-noise power ratio equal to unity, the background limited noise equivalent power,  $(NEP)_{BLIP}$  and the detectivity,  $D_{BLIP}^*$ , can be expressed as follows for n-type QWIPs.

$$(NEP)_{BLIP} = 2\sqrt{2h\nu BP_b/\eta} \quad (59)$$

$$D_{BLIP}^* = \sqrt{A_d B} / (NEP)_{BLIP} = \frac{\lambda_p}{2\sqrt{2}hc} \left( \frac{\eta}{Q_b} \right)^{1/2}, \quad (60)$$

where  $A_d$  is the active area of the detector, and  $Q_b = P_b / (Ah\nu)$  is the incident photon flux from the background for a given spectral bandwidth,  $\Delta\nu$ , and a peak wavelength,  $\lambda_p$ .  $Q_b$  is defined as

$$Q_b = \frac{2\pi}{c^2} \frac{\nu^2 \Delta\nu}{e^{h\nu/k_b T} - 1} \sin^2 \left( \frac{\theta}{2} \right), \quad (61)$$

where,  $\theta$ , is the field of view (FOV). For a p-type QWIP, a factor of  $\sqrt{2}$  is used in the denominator of Eq. (60),  $D_{BLIP}^*$ , since it can absorb both optical polarizations of the incident IR radiation.

## 2.3 Characterization of Strained Layer P-QWIPs

### 2.3.1 An $\text{In}_{0.4}\text{Ga}_{0.6}\text{As}/\text{GaAs}$ on GaAs P-QWIP with compressional strain

Unlike the  $\text{In}_{0.3}\text{Ga}_{0.7}\text{As}/\text{In}_{0.52}\text{Al}_{0.48}\text{As}$  on InP P-QWIP with tensile strain between the layers; which was reported on through the two previous semi-annual reports, a normal incidence  $\text{In}_{0.4}\text{Ga}_{0.6}\text{As}/\text{GaAs}$  on GaAs P-QWIP was designed for two color detection in the 3-5  $\mu\text{m}$  MWIR and 8-14  $\mu\text{m}$  LWIR bands. With this device, we have demonstrated two color detection in p-type strained-layer QWIPs for the first time.

The p-type compressively strained  $\text{In}_{0.4}\text{Ga}_{0.6}\text{As}/\text{GaAs}$  QWIP was grown on a semi-insulating (SI) GaAs substrate via molecular beam epitaxy (MBE). This QWIP structure consists of 20 periods of 40  $\text{\AA}$   $\text{In}_{0.4}\text{Ga}_{0.6}\text{As}$  quantum well Be-doped to a density of  $4 \times 10^{18} \text{ cm}^{-3}$  separated by a 350  $\text{\AA}$  wide barrier layer of undoped GaAs. A 0.3  $\mu\text{m}$  cap layer and a 1.0  $\mu\text{m}$  buffer layer of Be-doped GaAs with a dopant density of  $5 \times 10^{18} \text{ cm}^{-3}$  were grown to serve as top and bottom ohmic contacts. The contact and barrier layers are lattice

matched with the SI GaAs substrate, while the  $\text{In}_{0.4}\text{Ga}_{0.6}\text{As}$  quantum well layers are under biaxial compression with a designed lattice mismatch of approximately 2.8%. Due to the heavily doped large-bandgap contact layers of this P-QWIP, a large tunneling current from the triangle potential near the ohmic contact region may be dominant with respect to the QWIP's dark current. Therefore a relatively thick (550 Å) undoped GaAs barrier layer was grown next to the top and bottom contact layers to reduce this dark current component.

To facilitate the characterization of this P-QWIP, a  $200 \times 200 \mu\text{m}^2$  mesa structure was created by wet chemical etching. An Au/Cr film was deposited onto the QWIP mesas and the buffer layer via e-beam deposition with a thickness of approximately 1500 Å for ohmic contacts. The semi-insulating GaAs substrate was thinned down to approximately 50  $\mu\text{m}$  to lower the substrate absorption screening effect, and polished to a mirror-like surface to reduce the reflection of the normal incidence IR radiation.

Figures 2(a) and 2(b) show the idealized energy band diagram and energy subband states for the compressively strained P-QWIP. In this case, the intersubband transitions are from the highly populated heavy hole ground state ( $E_{HH1}$ ) to the upper heavy hole continuum states ( $E_{HH3}$  and  $E_{HH4}$ ) for the 8.9  $\mu\text{m}$  LWIR detection peak and the 5.5  $\mu\text{m}$  MWIR detection peak, respectively.

The mobility of the heavy-hole is enhanced by the compressive strain in the  $\text{In}_{0.4}\text{Ga}_{0.6}\text{As}$  quantum well due to the reduction of heavy hole effective mass by a factor of three<sup>31</sup>. Another effect attributed to the compressional strain localized in the quantum well is the decrease of the density of states in the well. This causes more heavy holes to reside in higher energy states, which effectively raises the Fermi level when compared with the same unstrained quantum well. The raised Fermi level will cause an increase in the number of off-center (i.e.,  $\mathbf{k} \neq 0$ ) free heavy holes with lighter effective mass; which in turn causes a larger intersubband absorption when exposed to normal incidence IR radiation. Our InGaAs/GaAs compressional strain P-QWIP has its heavy holes in type-I band alignment, while the light holes are in the type-II band configuration. The binary GaAs layer used as the barrier layer should also exhibit superior current transport characteristics when compared to a ternary barrier. Finally, the heavy hole excited continuum states are resonantly lined up with the light hole states; which gives rise to a strong quantum coupling effect. This resonant lined up effect makes the conducting holes behave like light holes. These resonant heavy holes

exhibit high mobilities, small effective masses, and long mean free paths. Therefore, larger photoconductive gain and higher photoconductivity are expected for a compressively strained P-QWIP when compared with an unstrained one.

When compared with the  $\text{In}_{0.3}\text{Ga}_{0.7}\text{As}/\text{In}_{0.52}\text{Al}_{0.48}\text{As}$  tensile strain P-QWIP and the new InGaAs/AlGaAs compressive strain P-QWIP, the measured dark current at various temperatures is much higher. This device also exhibits an asymmetrical dark current characteristic (figure 6), like the InGaAs/InAlAs tensile strain P-QWIP, which can be attributed to the dopant migration effect which occurs during layer growth<sup>32</sup>. For a field of view (FOV) of 90° the InGaAs/GaAs compressionally strained P-QWIP is under background limited performance (BLIP) at  $V_b = 0.3$  V,  $T = 70$  K and  $V_b = 0.7$  V,  $T = 55$  K.

The responsivity of this QWIP was measured under normal incidence illumination as a function of temperature, applied bias, and incident IR wavelength using a blackbody radiation source and automatic PC-controlled single grating monochrometer system. Twin LWIR peaks were detected at  $\lambda_{p1} = 8.9$   $\mu\text{m}$  and  $\lambda_{p2} = 8.4$   $\mu\text{m}$  as shown in figure 3(a). A single MWIR peak was discovered at  $\lambda_{p3} = 5.5$   $\mu\text{m}$  as seen in figure 3(b). At each peak wavelength, responsivities were measured as 24 mA/W at  $V_b = 0.3$  V and 45 mA/W at  $V_b = 0.7$  V for  $T \leq 75$  K. The twin LWIR peaks covered a broad wavelength band ranging from 6.5 to 12  $\mu\text{m}$ . The cut-off wavelength for the LWIR band was found to be  $\lambda_c \approx 10$   $\mu\text{m}$ , which corresponds to a spectral bandwidth of  $\Delta\lambda/\lambda_p = 35\%$ . The twin peak wavelengths are attributed to the intersubband transition from the confined ground heavy hole state ( $E_{HH1}$ ) to the continuum heavy hole states ( $E_{HH3}$ ), which is resonantly lined up with the type-II light hole continuum states. The transition energies for the 8.9  $\mu\text{m}$  and 8.4  $\mu\text{m}$  peak wavelengths are in reasonable agreement with our theoretical calculations. While the physical origins of the twin LWIR peaks is not clear, a possible explanation can be given as follows. When the HH and LH bands in the continuum are strongly mixed, either individual subband can further split into two sub-subbands due to coupling or interaction, with one shifting up in energy and the other shifting down in energy. This gives rise to the observed twin detection peaks in the LWIR band. The MWIR peak observed at 5.5  $\mu\text{m}$  had a wavelength bandwidth ranging from 4 to 6.5  $\mu\text{m}$ . The measured responsivities of the MWIR band were found to be 7 mA/W and 13 mA/W at  $V_b = 0.3, 0.7$  V and  $T = 75$  K, respectively. The spectral bandwidth of  $\Delta\lambda/\lambda_{p3} = 27\%$  was obtained with the cut-off wavelength at  $\lambda_c = 6$   $\mu\text{m}$ . The

MWIR detection is attributed to the intersubband transition between the ground heavy hole state ( $E_{HH1}$ ) and the upper continuum heavy hole state ( $E_{HH4}$ ). In this case, no mixing or interaction between the HH and LH subbands was observed. A probable explanation is that the weak overlap interaction at higher subband levels prevents the sub-subband formation.

Responsivities for this compressively strained P-QWIP were measured at  $T = 75$  K, and the results are shown in figures 4 and 5. The responsivity of the twin peak (either  $\lambda_{p1} = 8.9 \mu\text{m}$  or  $\lambda_{p2} = 8.4 \mu\text{m}$ ) LWIR band increases almost linearly with bias voltage for  $V_b \geq -1.6$  V and  $V_b \leq +1.2$  V. A similar photoresponse was obtained for the detective peak at  $\lambda_{p3} = 5.5 \mu\text{m}$ , as shown in figure 9(b). The gain has a maximum value of 0.13 at  $V_b = 1.6$  V. The linear photoresponse exhibited by this device is due to the photoconductive gain which varies linearly with bias. The maximum gain,  $G = 0.13$ , is the highest value ever reported in a P-QWIP.

### 2.3.2 An InGaAs/AlGaAs on GaAs P-QWIP with compressive strain layers

A new compressively strained p-QWIP loosely based on the InGaAs/GaAs on SI GaAs was designed using the InGaAs/AlGaAs system for the quantum well/barrier structures, which was grown on semi-insulating GaAs. With this new structure, we have demonstrated the continued viability and flexibility of the p-type compressive strain QWIP system. This structure exhibits the lowest dark current obtained with a p-type compressive strain QWIP to date, and exhibits excellent uniformity with respect to staring focal plane array use.

The new p-type compressively strained QWIP was grown on a semi-insulating GaAs substrate by molecular beam epitaxy. This QWIP consists of 20 periods of  $\text{In}(y \approx 0.2)\text{GaAs}$  quantum wells of roughly  $40 \text{ \AA}$  in width p-doped to a density of approximately  $2 \times 10^{18} \text{ cm}^{-3}$ , separated by approximately  $500 \text{ \AA}$  wide undoped  $\text{Al}(x \approx 0.15)\text{GaAs}$  barriers. A  $0.3 \mu\text{m}$  cap layer and a  $1.0 \mu\text{m}$  buffer layer of p-doped AlGaAs with a dopant density of  $5 \times 10^{18} \text{ cm}^{-3}$  were also grown to serve as top and bottom ohmic contacts. The contact and barrier layers are roughly lattice matched to the SI GaAs substrate so that the InGaAs quantum wells are in biaxial compression with a designed lattice mismatch of nearly -1.4 %. Since the top and bottom contact layers are formed from heavily doped, large bandgap materials, a large tunneling current from the triangle potential near these ohmic contact regions may dominate the dark current of the QWIP. Therefore, rather thick undoped barrier layers

of AlGaAs were grown between the contact layers and the QWIP structure to reduce this component of the dark current. A schematic diagram of this structure is shown in figure 7. The LWIR hole transition after absorption was designed to be from the heavy hole ground state (HH1) to the third heavy hole state (HH3), which is in resonance with the AlGaAs barrier. The MWIR transition is speculated to arise from the same heavy hole ground state to the next higher (HH4) extended state.

Again, to facilitate the characterization of this compressively strained p-QWIP, a  $200 \times 200 \mu\text{m}^2$  mesa was etched onto the wafer by wet chemical etching. After patterning via a contact mask, a thin film of approximately  $1200 \text{ \AA}$  of Au/Cr was deposited onto the mesa top contact and bottom buffer contact layers via e-beam deposition at a relatively slow rate for ohmic contacts. For this sample, the semi-insulating GaAs substrate was not thinned for ease of handling and simplification of the processing steps. Although this does lower the effective quantum efficiency of the device, by only letting the incident radiation have one pass through the quantum well layers. Future studies will utilize the backside thinning and a reflective top contact to enhance the effective quantum efficiency and therefore improve the p-QWIP's performance.

Figure 8 shows the dark current characteristic of the InGaAs/AlGaAs compressively strained p-QWIP. When compared with the dark current characteristics of the previous compressively strained p-QWIP with a LWIR peak at  $\lambda = 8.9 \mu\text{m}$ , at similar device temperatures, the dark current for the new p-QWIP is roughly two orders of magnitude lower (see also figure 6). As can be clearly seen in this figure, the device is under background limited photocurrent (BLIP) conditions at temperatures of less than 63 K for applied biases of up to  $\pm 3 \text{ V}$  with BLIP temperatures of up to 70 K possible at biases of lower than approximately 1 V. When compared with the dark current characteristic of the previously studied tensile strain p-QWIP, the dark current in the compressively strained InGaAs/AlGaAs p-QWIP is still higher. Like all of the previously studied p-QWIPs, the dark current characteristic is slightly asymmetric. This can be attributed to the doping migration effect as which occurs during layer growth, as previously explained<sup>32</sup>.

Again, in this p-QWIP, the mobility of the heavy-holes are enhanced by the compressive strain in the InGaAs quantum well due to the reduction of the heavy hole effective mass by a factor of three<sup>31</sup>. Another effect that is attributed to the compressional strain localized in

the quantum well layer is the decrease in the density of states in the well. This phenomenon causes more heavy holes to reside in higher energy states, the net effect of which is to raise the Fermi level inside the quantum well when compared to the unstrained state. This effect not only causes an increase in the number of off-center ( $k \neq 0$ ) free heavy holes with lighter effective mass, which in turn causes a larger intersubband absorption when exposed to normal incidence IR radiation; but it also reduces the effective doping needed in the quantum well, so that the dark current is similarly reduced.

The responsivity of this p-QWIP was measured under normal incidence illumination as a function of temperature, applied bias, and incident IR radiation by using a blackbody radiation source running through an automatic PC-controlled single grating monochrometer with the appropriate filters attached. A single LWIR peak was detected at  $\lambda_p = 7.4 \mu\text{m}$  at liquid nitrogen ( $\text{LN}_2$ ) temperatures ( $T = 77 \text{ K}$ ) and under an applied bias of 5 V, as shown in figure 10. A single MWIR peak was discovered at  $\lambda_p = 5.5 \mu\text{m}$  under the same conditions as previously mentioned, and is shown in figure 12. The respective responsivities for the LWIR and MWIR peaks were found to be 38 mA/W and 8 mA/W. The LWIR band is rather broad as illustrated in figure 10, with a cut-off wavelength of  $\lambda_c \approx 10 \mu\text{m}$ , which corresponds to a half-peak spectral bandwidth of  $\Delta\lambda/\lambda_p = 30 \%$ . The asymmetrical responsivity around the spectral peak is attributed to the long-pass filter characteristic, which has a cut-on at  $\lambda = 6.7 \mu\text{m}$ . In figure 9, we see the peak responsivity measured as a function of bias and device temperature. As clearly seen in this figure, the responsivity is linearly proportional to the applied bias and that the variation with temperature is minimal. The MWIR peak at  $\lambda_p = 5.5 \mu\text{m}$  has an approximate wavelength bandwidth ranging from 4 to  $6.5 \mu\text{m}$ , which overlaps with the expected bandwidth of the  $7.4 \mu\text{m}$  peak. For a cut-off wavelength of  $6 \mu\text{m}$ , a spectral bandwidth of  $\Delta\lambda/\lambda_p = 27 \%$  was obtained. Again, the responsivity as a function of bias was measured and a linear relation was found.

## 2.4 Conclusion and Remarks

Over the last half-year period, we have achieved a greater understanding in regards to the design and characterization of P-QWIPs. We previously demonstrated a novel strained-layer design that utilizes biaxial tension on an InP substrate with ultra-low dark current, high detectivity, high responsivity, and BLIP operation. We have also demonstrated a re-

liable, novel compressively strained-layer design on a GaAs substrate with two color BLIP operation in the MWIR and LWIR bands, high detectivity, high responsivity, and high gain. The current p-QWIP under investigation can be characterized as a reliable evolution of the previous compressively strained p-QWIP with lower dark current and similar spectral characteristics, albeit at a shorter wavelength; but again with two-color detection in the LWIR and MWIR bands. Efforts are being made to maintain the dark current levels at their current low values or even lower them while extending the detective peaks of the p-QWIPs further into the LWIR band, near the  $10 \mu\text{m}$  range.

## References

1. B. F. Levine, R. J. Malik, J. Walker, K. K. Choi, C. G. Bethea, D. A. Kleinman, and J. M. Vandenberg, *Appl. Phys. Lett.* **50**, 273 (1987).
2. L. S. Yu, S. S. Li, *Appl. Phys. Lett.* **59**, 1332 (1991).
3. G. Hasnain, B. F. Levine, C. G. Bethea, R. A. Logan, J. Walker, and R. J. Malik, *Appl. Phys. Lett.* **54**, 2515 (1989).
4. J. Y. Andersson and L. Lundqvist, *J. Appl. Phys.* **71**, 3600 (1992).
5. B. F. Levine, S. D. Gunapala, J. M. Kuo, S. S. Pei, and S. Hui, *Appl. Phys. Lett.* **59**, 1864 (1991).
6. J. Katz, Y. Zhang, and W. I. Wang, *Electron. Lett.* **28**, 932 (1992).
7. W. S. Hobson, A. Zussman, B. F. Levine, and J. deJong, *J. Appl. Phys.* **71**, 3642 (1992).
8. J. W. Matthews and A. E. Blakeslee, *J. Cryst. Growth* **32**, 265 (1976).
9. Landolt-Bornstein, "Numerical Data and Functional Relationships in Science and Technology", O. Madelung, ed., Group III, **17a**, **22a**, Springer-Verlag, Berlin (1986).
10. G. Ji, D. Huang, U. K. Reddy, T. S. Henderson, R. Houre, and H. Morkoç, *J. Appl. Phys.* **62**, 3366 (1987).
11. T. P. Pearsall, *Semiconductors and Semimetals*, **32**, 55 (1990).
12. H. Asai, and Y. Kawamura, *Appl. Phys. Lett.* **56**, 746 (1990).
13. H. Xie, J. Katz, and W. I. Wang, *Appl. Phys. Lett.* **59**, 3601 (1991).
14. R. T. Kuroda and E. Garmire, *Infrared Phys.* **34**, 153 (1993).
15. L. R. Ram-Mohan, K. H. Yoo, and R. L. Aggarwal, *Phys. Rev B* **38**, 6151 (1988).
16. J. M. Luttinger and W. Kohn, *Phys. Rev.* **97**, 869 (1956).

17. J. M. Luttinger, *Phys. Rev.* **102**, 1030 (1956).
18. G. L. Bir and G. E. Pikus, "Symmetry and Strain-Induced effects in Semiconductors", Wiley, New York (1974).
19. E. L. Derniak and D. G. Crowe, *Optical Radiation Detectors*, Wiley, New York (1984).
20. B. F. Levine, C. G. Bethea, G. Hasnain, J. Walker, and R. J. Malik, *Appl. Phys. Lett.* **53**, 296 (1988).
21. D. A. Scribner, M. R. Kruer, and J. M. Killiany, *Proc. of the IEEE* **79**, 66, (1991).
22. R. Hull, J. C. Bean, F. Cerdeira, A. T. Fiory, and J. M. Gibson, *Appl. Phys. Lett.* **48**, 56 (1986).
23. E. O. Kane, "Semiconductors and Semimetals", eds. R. K. Willardson and A. C. Bear, **1**, 75 (1966).
24. F. H. Pollack, "Semiconductors and Semimetals", ed. T. P. Pearsall, **32**, 17 (1990).
25. Y. C. Chang and R. B. James, *Phys Rev.* **B-39**, 672 (1989).
26. P. Man and D. S. Pan, *Appl. Phys. Lett.* **61**, 2799 (1992).
27. S. K. Chun, D. S. Pan, and K. L. Wang, *Phys. Rev.* **B-47**, 15638 (1993).
28. B. F. Levine, *J. Appl. Phys.* **74**, R1 (1993).
29. J. W. Matthews and A. E. Blakeslee, *J. Cryst. Growth* **27**, 118 (1974).
30. J. W. Matthews and A. E. Blakeslee, *J. Cryst. Growth* **29**, 273 (1975).
31. K. Hirose, T. Mizutani, and K. Nishi, *J. Cryst. Growth* **81**, 130 (1987).
32. H. C. Liu, Z. R. Wasilewski, and M. Buchanan, *Appl. Phys. Lett.* **63**, 761 (1993).
33. A. K. Ghatak, K. Thyagarajan, and M. R. Shenoy, *IEEE J. Quantum Electron.* **24**, 1524 (1988).
34. H. C. Liu, *Appl. Phys. Lett.* **60**, 1507 (1992).

35. H. C. Liu, *Appl. Phys. Lett.* **61**, 2703 (1992).
36. W. A. Beck, *Appl. Phys. Lett.* **63**, 3589 (1993).
37. S. D. Gunapala, B. F. Levine, and K. West, *J. Appl. Phys.* **69**, 6517 (1991).

<i>Device</i> (strain)	$\lambda_p$ $\mu\text{m}$	<i>Responsitivity</i> (mA/W)	<i>Dark Current</i> (A) @ 77 K, 1 V
InGaAs/InAlAs (tensile)	8.1	18	$5 \times 10^{-8} \text{ A/cm}^2$
InGaAs/GaAs (compressive)	8.9, 8.4, 5.5	45	$1 \times 10^{-5}$
InGaAs/AlGaAs (compressive)	7.4, 5.5	38	$5 \times 10^{-8}$

**Table 1.** Comparison of the strained layer p-QWIPs studied so far.

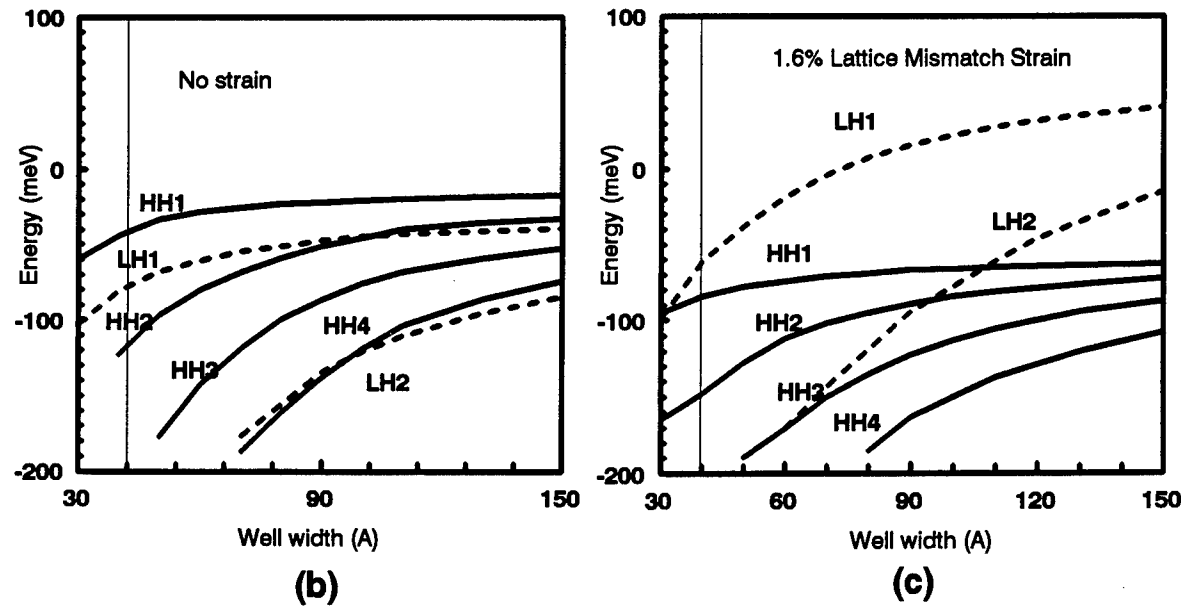
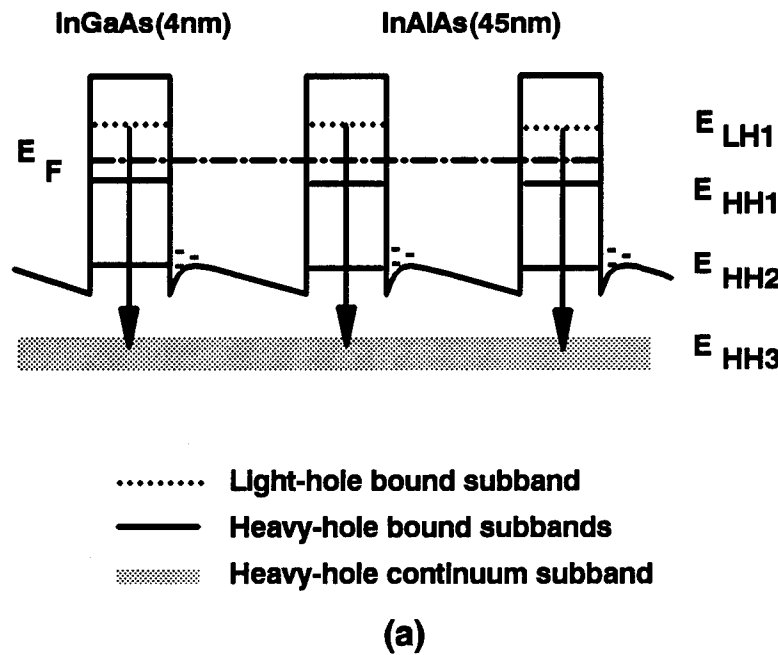
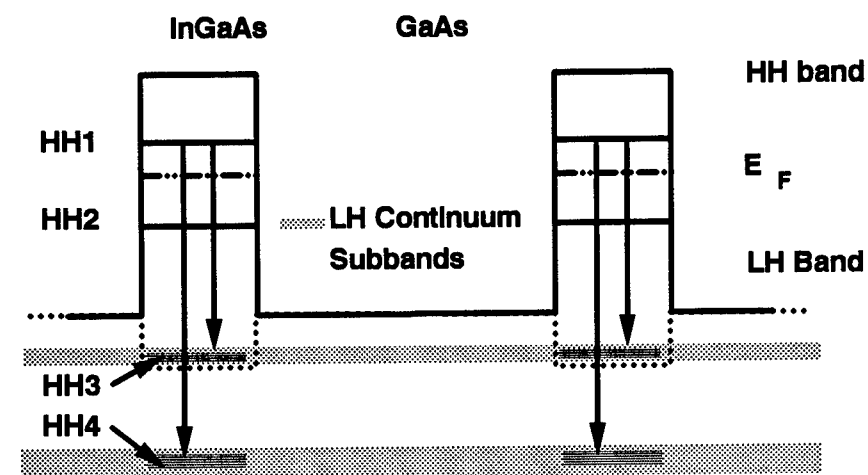
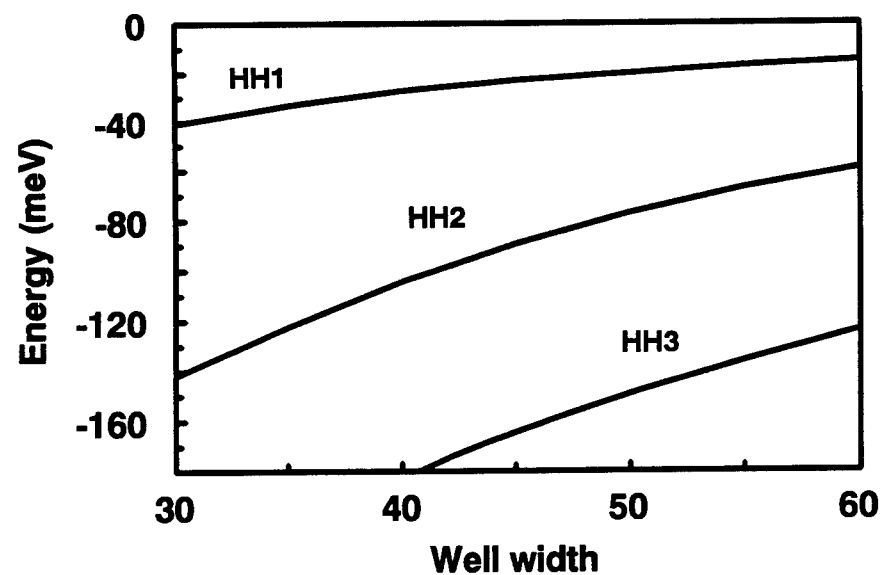


Figure 1: Schematic of the tensile strain-layer InGaAs/InAlAs on InP p-QWIP (a) with the unstrained band calculations (b) and the strain-layer band calculations (c).



(a)



(b)

Figure 2: Schematic of the compressive strain layer InGaAs/GaAs on GaAs p-QWIP (a) and the strain-layer energy band calculations (b).

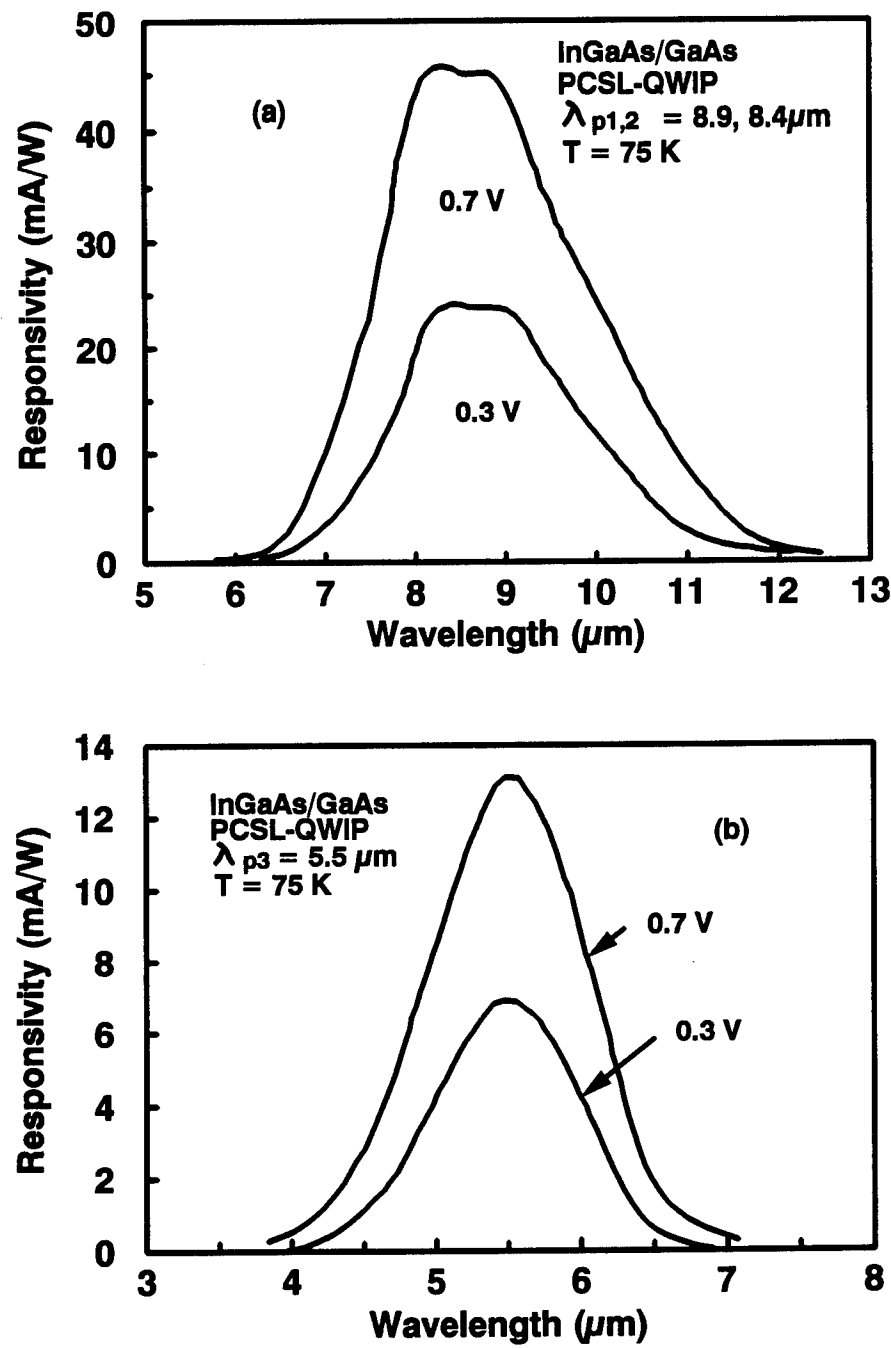


Figure 3: Measured responsivities in the LWIR band (a) and the MWIR band (b) for the InGaAs/GaAs PCSL-QWIP.

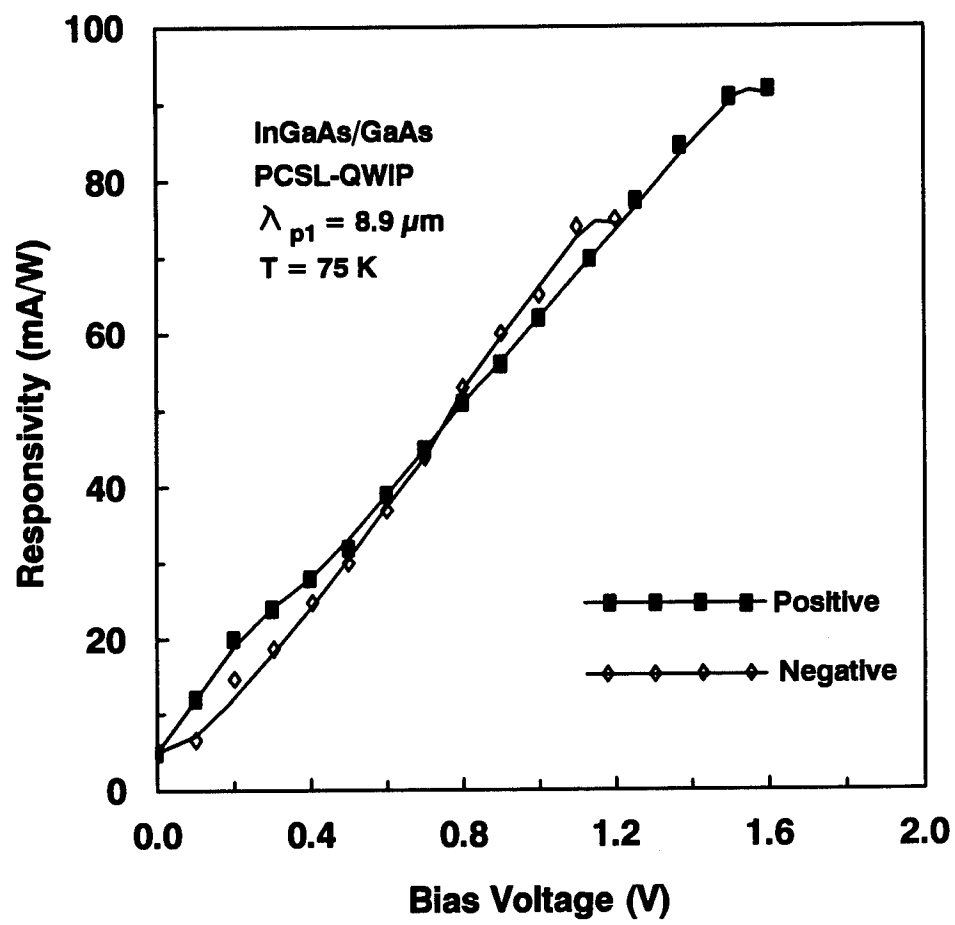


Figure 4: Measured responsivity of the InGaAs/GaAs PCSL-QWIP as a function of applied bias for  $\lambda_p = 8.9 \mu\text{m}$ .

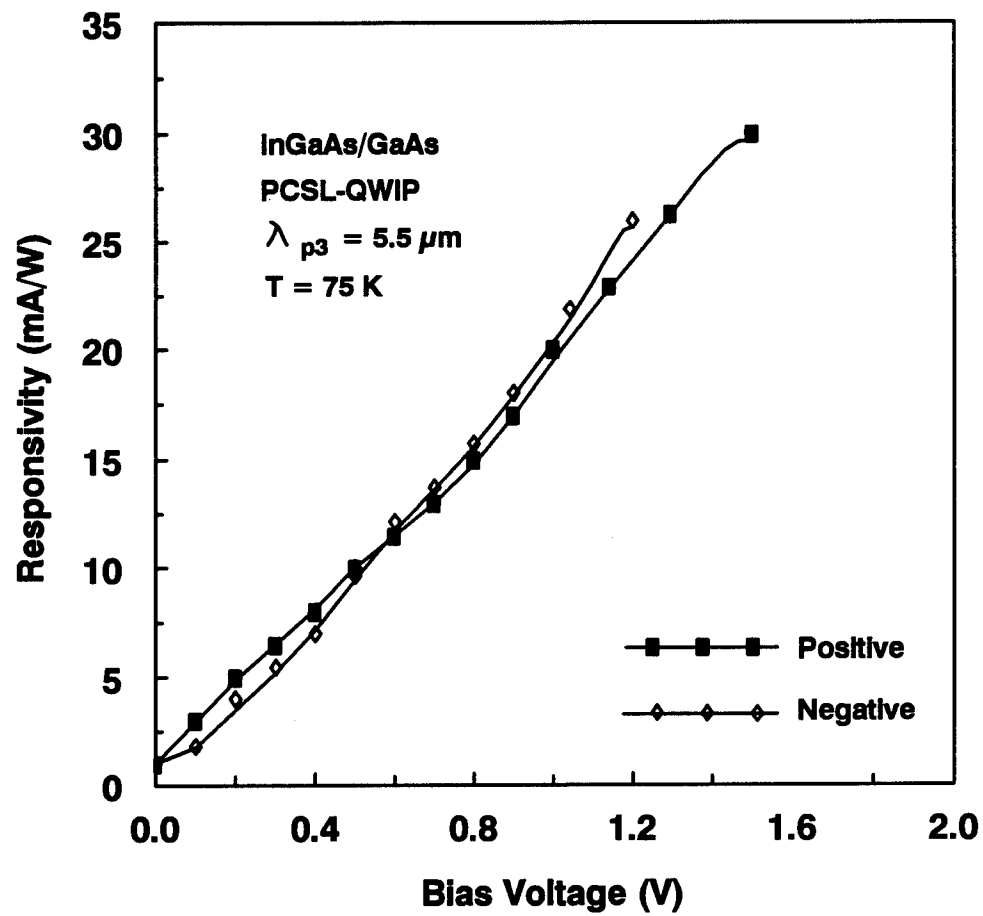


Figure 5: Measured responsivity of the InGaAs/GaAs PCSL-QWIP as a function of applied bias for  $\lambda_p = 5.5 \mu\text{m}$ .

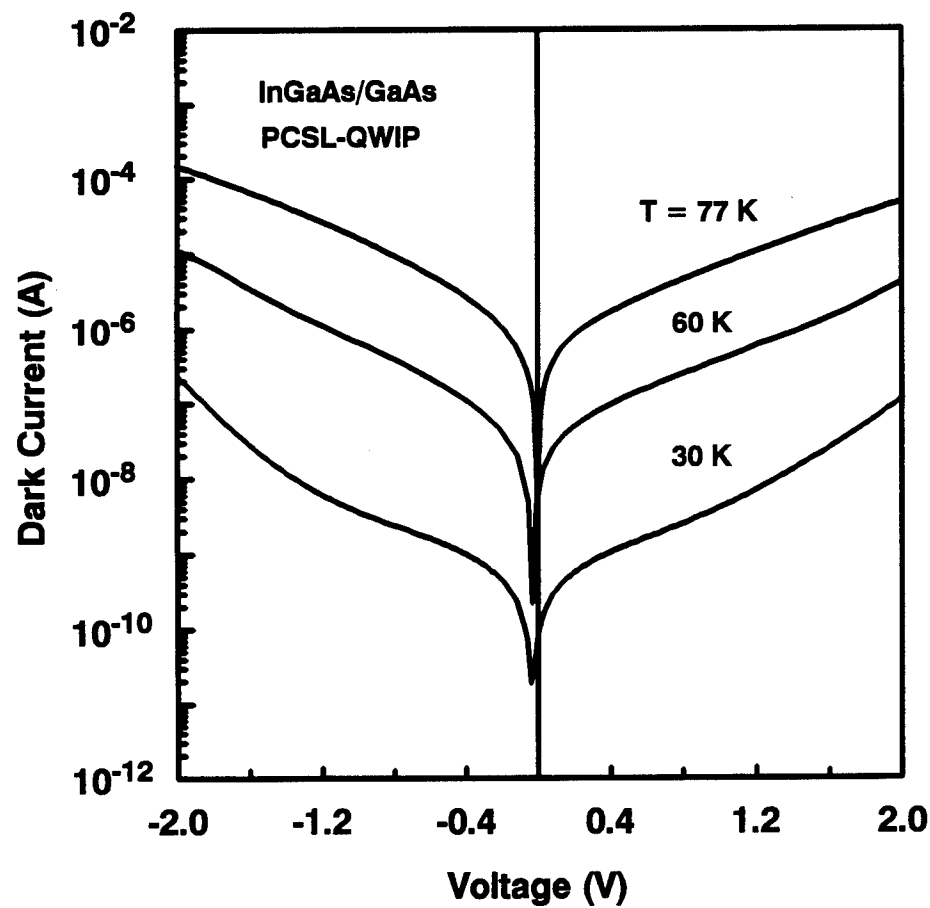


Figure 6: Measured dark current for the InGaAs/GaAs PCSL-QWIP as a function of applied bias and device temperature.

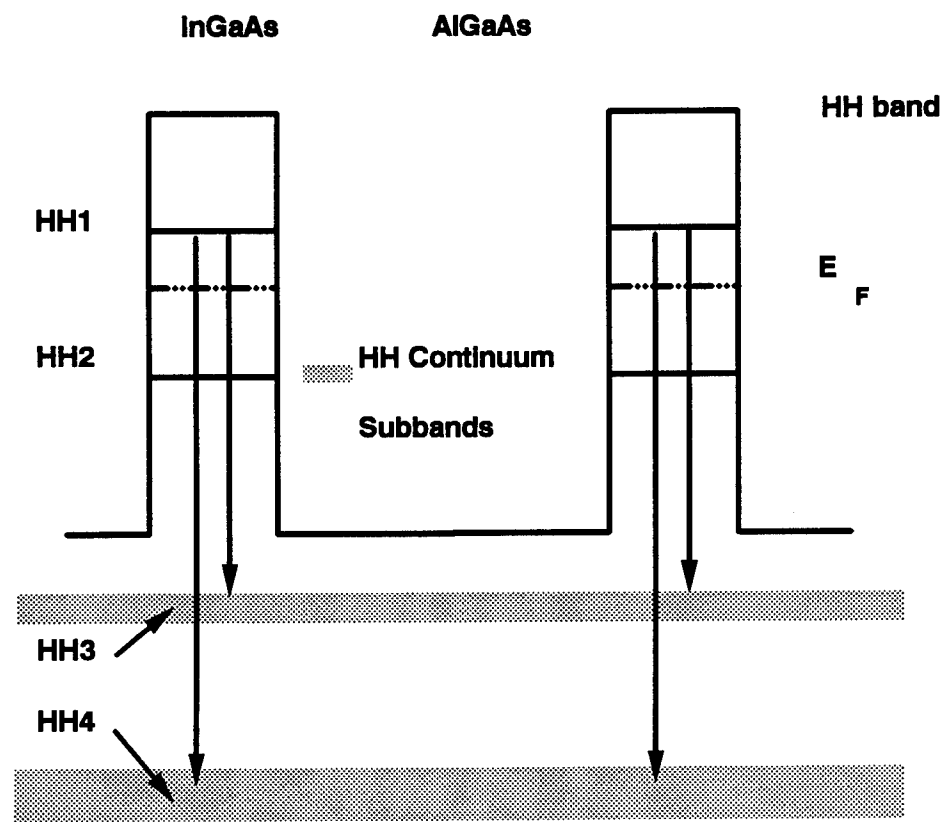


Figure 7: Schematic of the InGaAs/AlGaAs on GaAs p-QWIP.

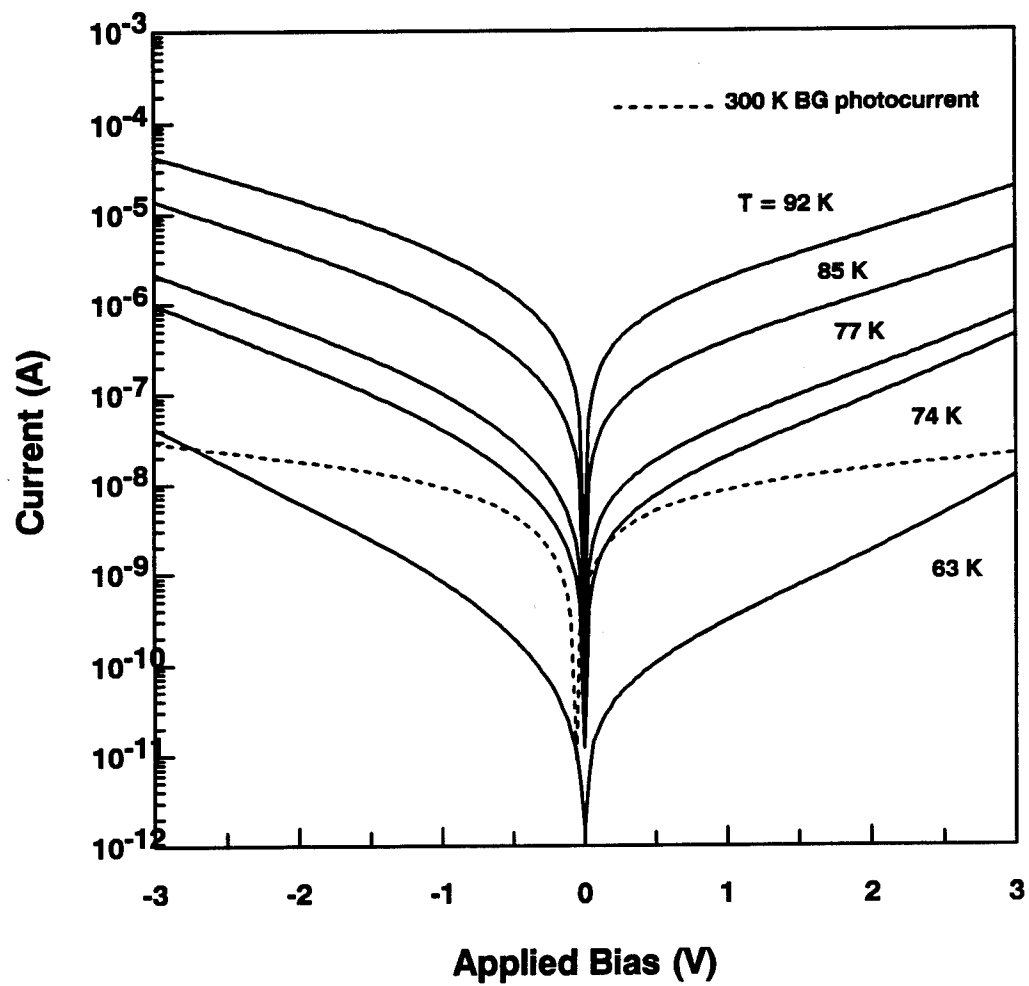


Figure 8: Measured dark current for the InGaAs/AlGaAs PCSL-QWIP as a function of applied bias and device temperature with the 300 K background photocurrent superimposed.

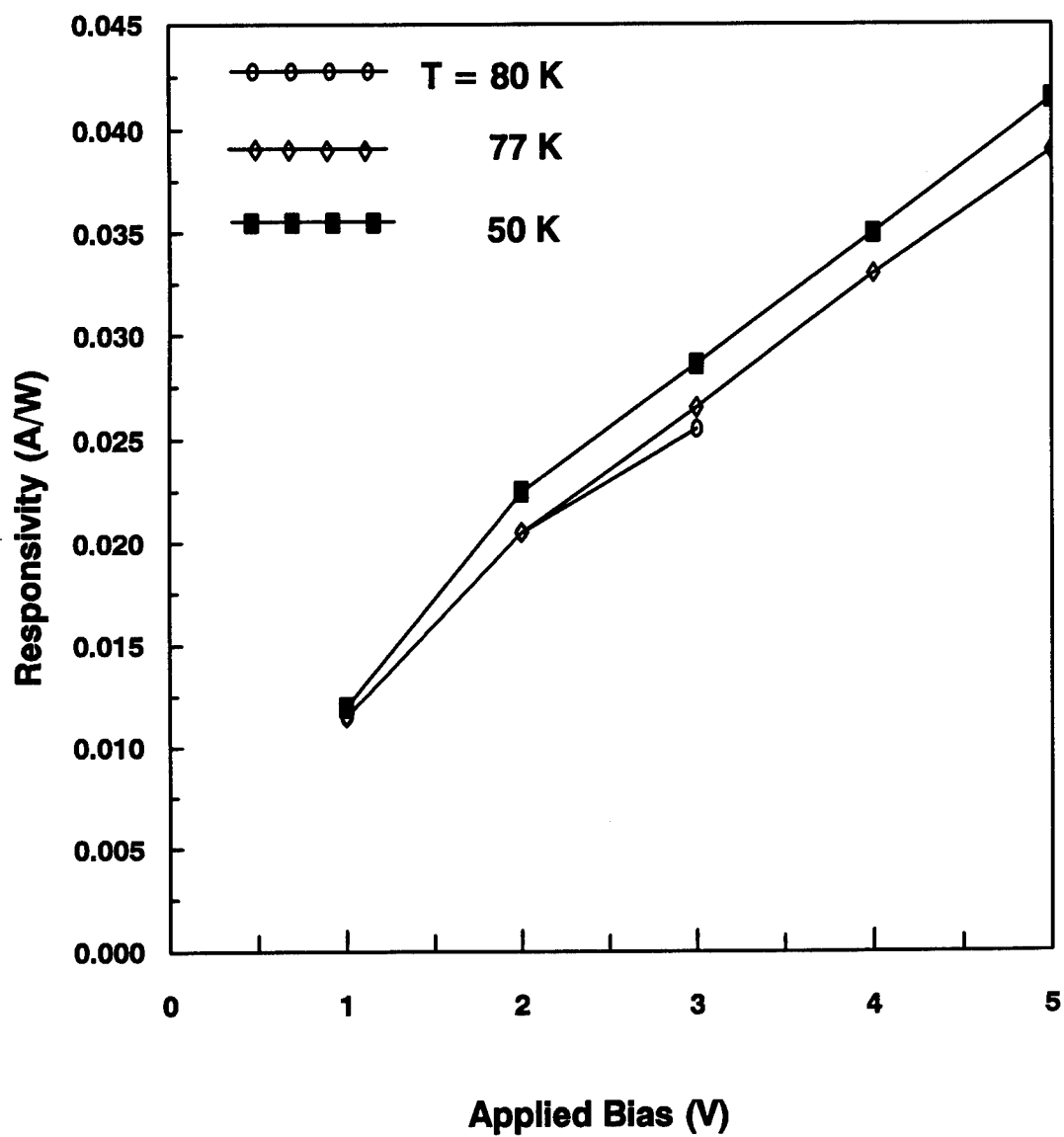


Figure 9: Measured responsivity as a function of applied bias and device temperature for the InGaAs/AlGaAs PCSL-QWIP at  $\lambda_p = 7.4 \mu\text{m}$ .

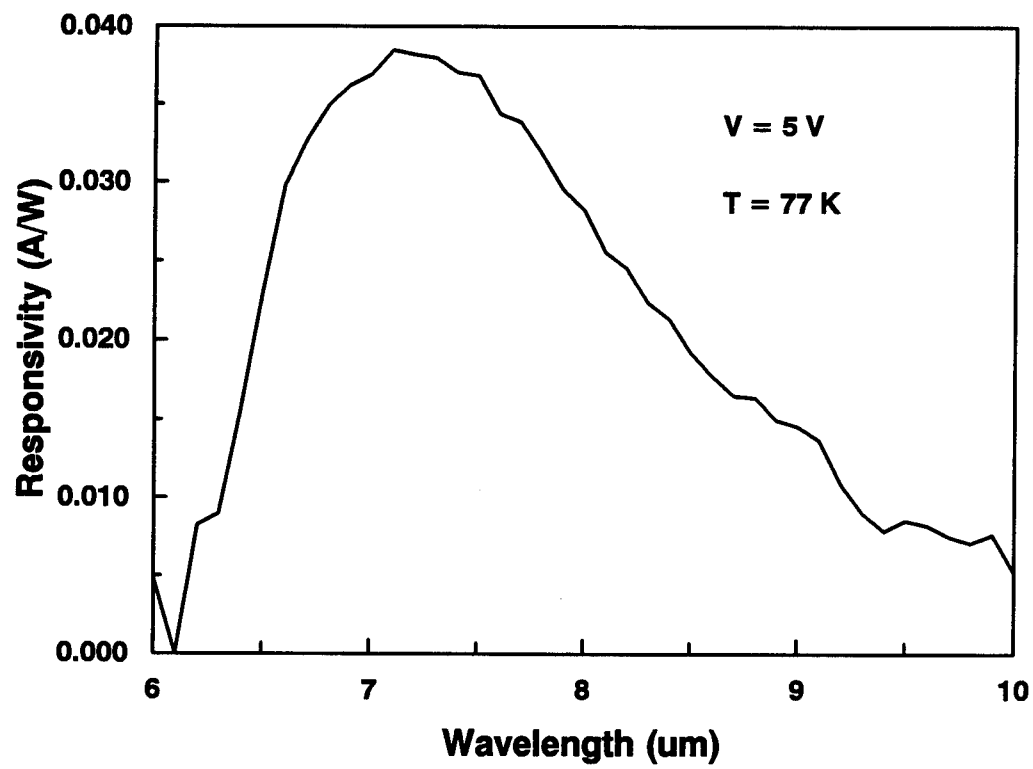


Figure 10: Calculated responsivity as a function of incident radiation wavelength in the LWIR band.

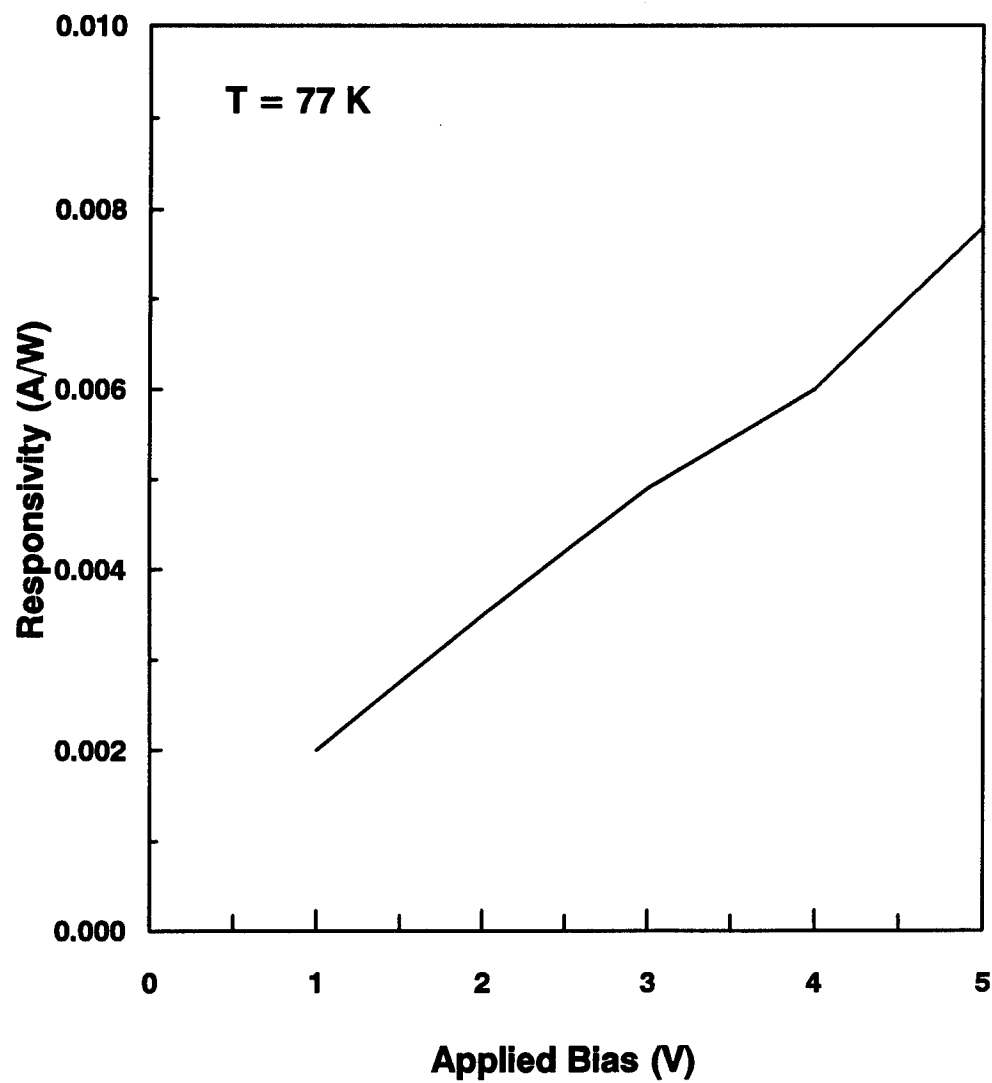


Figure 11: Measured responsivity as a function of applied bias of the InGaAs/AlGaAs PCSL-QWIP at  $\lambda_p = 5.5\text{ }\mu\text{m}$ .

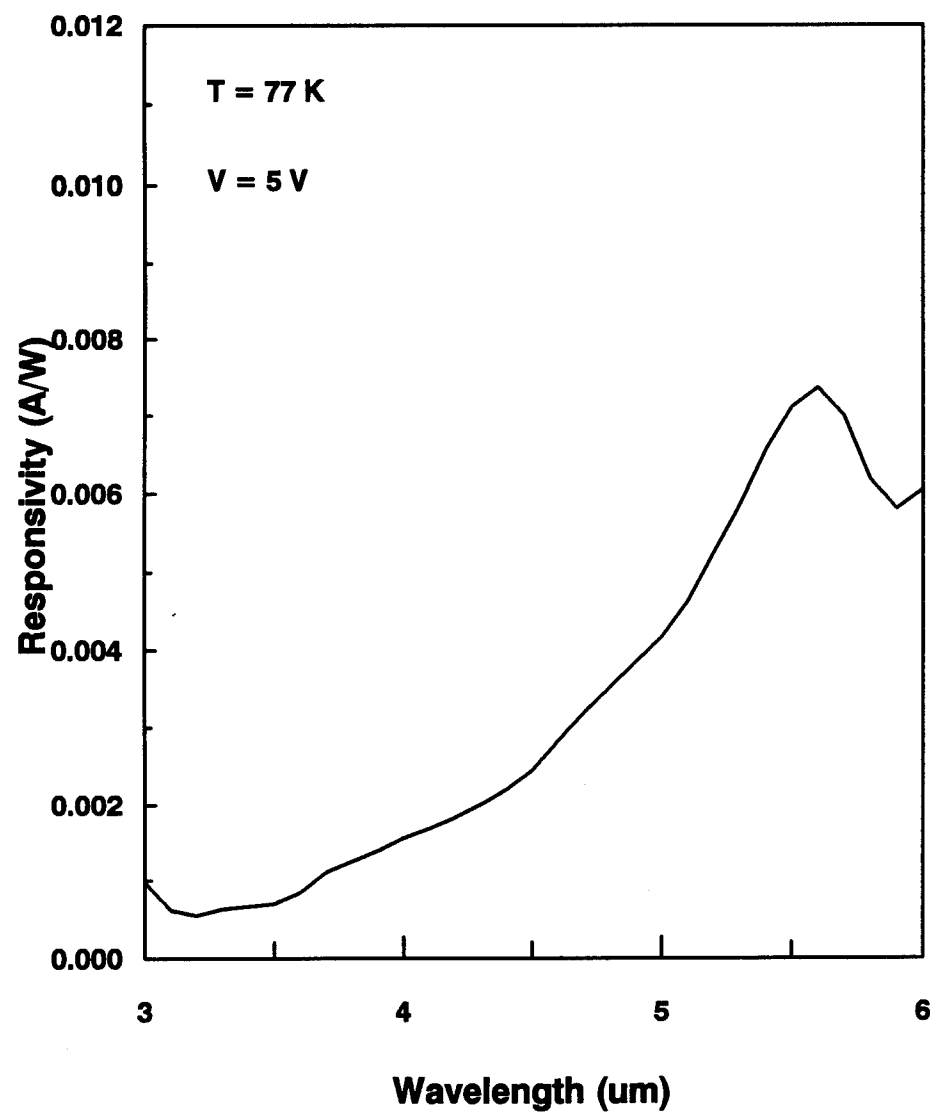


Figure 12: Calculated responsivity as a function of incident radiation wavelength in the MWIR band.

REPORT DOCUMENTATION PAGE			Form Approved OMB No. 0704-0188
<small>Public reporting burden for this collection of information is estimated to average 1 hour per response, including the time for reviewing instructions, searching existing data sources, gathering and maintaining the data needed, and completing and reviewing the collection of information. Send comments regarding this burden estimate or any other aspect of this collection of information, including suggestions for reducing this burden, to Washington Headquarters Services, Directorate for Information Operations and Reports, 1215 Jefferson Davis Highway, Suite 1204, Arlington, VA 22202-4302, and to the Office of Management and Budget, Paperwork Reduction Project (0704-0188), Washington, DC 20503.</small>			
1. AGENCY USE ONLY (Leave blank)	2. REPORT DATE 15 Feb. 1995	3. REPORT TYPE AND DATES COVERED Progress Report: 07/16/94-02/15/95	
4. TITLE AND SUBTITLE Investigation of a Normal Incident High Performance P-type Strained Layer In <sub>0.3</sub> Ga <sub>0.7</sub> As/In <sub>0.52</sub> Ga <sub>0.48</sub> As Quantum Well Infrared Photodetector			5. FUNDING NUMBERS ONR #N00014-93-1-0827
6. AUTHOR(S) Jerome T. Chu, Student Sheng S. Li, Professor			
7. PERFORMING ORGANIZATION NAME(S) AND ADDRESS(ES) University of Florida Gainesville, FL 32611-6200			8. PERFORMING ORGANIZATION REPORT NUMBER 92120712
9. SPONSORING / MONITORING AGENCY NAME(S) AND ADDRESS(ES) US Navy, Office of Naval Research 800 North Quincy Street, Code 1512B:SM Arlington, VA 22217-5000			10. SPONSORING / MONITORING AGENCY REPORT NUMBER
11. SUPPLEMENTARY NOTES			
12a. DISTRIBUTION / AVAILABILITY STATEMENT Approved for public release, distribution unlimited.		12b. DISTRIBUTION CODE	
13. ABSTRACT (Maximum 200 words) During this reporting period, we have made excellent progress towards the program goals. A significant achievement was made in the development of a new compressionally strained p-type GaAs/InGaAs QWIP grown on GaAs by MBE. This new QWIP achieved two color detection with detective peaks at 8.9 μm and 8.4 μm in the LWIR band and 5.5 μm in the MWIR band. This detector is under background limited performance (BLIP) at temperatures up to 70 K. The measured responsivity were found to be 24 mA/W and 45 mA/W for the two LWIR peaks respectively, while a responsivity of 13 mA/W was found for the MWIR peak; all at T=75 K. In addition, a new InGaAs/AlGaAs on GaAs compressionally strained p-QWIP was developed which exhibits extremely low dark currents and comparable responsivities when compared with the previous PCSL-QWIP. The measured responsivity was found to be 38 mA/W and 8mA/W at T=77 K, with the detective peaks at 7.4 and 5.5 μm, respectively. The detector is under BLIP conditions at T=63 K with applied biases from -3 V to +3 V.			
14. SUBJECT TERMS P-type strained layer InGaAs/GaAs quantum well infrared photodetectors (QWIPs), intersubband absorption, dark current, responsivity, detectivity.			15. NUMBER OF PAGES
			16. PRICE CODE
17. SECURITY CLASSIFICATION OF REPORT Unclassified	18. SECURITY CLASSIFICATION OF THIS PAGE	19. SECURITY CLASSIFICATION OF ABSTRACT	20. LIMITATION OF ABSTRACT Unlimited